

May 26, 2017



A Review of Noise Modes and Benefits and Detriments of Arrays

Who Should Read this Treatise

If you work with seismic data, this document may be of interest to you. If you work with planning and execution of seismic projects, you should certainly read it. If you do not know what is meant by “chaotically-scattered noise” then you should definitely read it. If you think that arrays of analog geophones should **always** be used or if you think that arrays of analog geophones should **never** be used, then you should definitely read it. If you think that groups of several geophones should always be “podded” or if you think that point-receivers should always be used at the relatively sparse intervals we have used in the past, then you absolutely must read this.

Since the advent of digital single-point sensors in the early 1990’s there has been a preponderance of discussions, workshops and publications regarding the use of analog arrays versus point receivers (both digital and analog). The release of Western Geophysical’s Q-Land system in 2000 further proliferated these discussions. The conclusions that are proffered by these studies are not always consistent.

The confusion is partly due to the natural desire of geophysicists to have a simple answer. Should arrays be used or not? Unfortunately, the reflection seismic method is not simple to implement in a real world. We must deal with some constrained variables and many unconstrained variables and all must be considered before reaching conclusions.

In this document we attempt to illustrate various types of noise that are encountered in seismic projects and we discuss the relative severity of each. We describe the concept of sub-sampling as a tool to extend the sampling Nyquist and avoid contamination of our desired signals with short wavelength noise modes. We compare sub-sampling achieved by the use point-receivers and point-sources in small spatial sample intervals versus the use of analog arrays. We address several advantages and disadvantages of each method. We also clarify some concepts about trace density and how it may best be achieved. More detail on this topic will be addressed in our next paper (currently being prepared).

Table of Contents

Who Should Read this Treatise	1
Table of Contents	2
One Simple Answer	2
Noise Modes and Characteristics	6
Random Noise	6
Erratic Noise	8
Noise due to Irregular Source Behavior	9
Coherent Source-Generated Noise	11
Chaotically-Scattered Source-Generated Noise	16
Sub-Sampling of Noise	25
Sub-Sampling in the Source Domain using Arrays	27
Arrays and Sub-Sampling in the 2D CDP Domain	33
Arrays and Sub-Sampling in 3D	41
Increasing Trace Density by Reducing Line Spacing in 3D	44
Final Comments	50

One Simple Answer

One simple answer comes from consideration of an ideal situation. Using simple geologic models of typical target reservoirs where we introduce a controlled source wavelet, we can easily calculate the character of reflections as observed by receivers deployed along a flat surface.

We talk about the rate of change of vertical particle velocity along the receiving surface (wavenumber) or the inverse which we call “apparent wavelength” of the signal. This is simply a measure of how rapidly our desired signals change in space along the surface where the receivers are located. As shown in figure 1, the apparent wavelength (λ_{app}) is a function of source-receiver offset (X), depth to reflector (D), frequency of wavelet oscillation (F) and velocity of wavelet propagation (V).

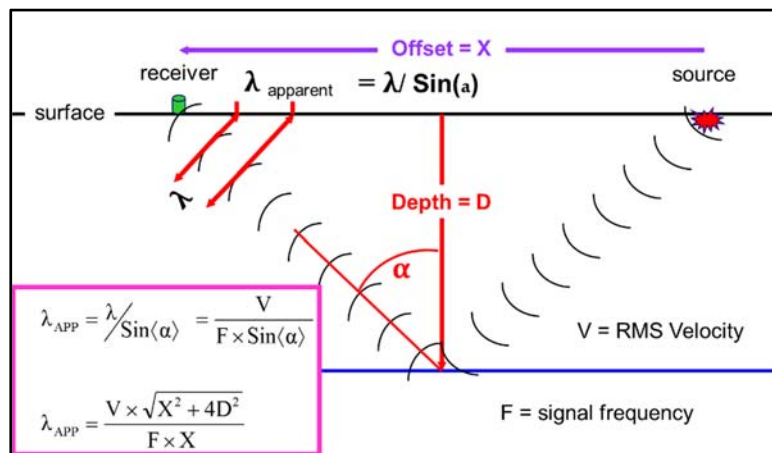


Figure 1. A simple model with flat surface, flat reflector and material between that is homogeneous and isotropic. We can see that the apparent wavelength of reflected signal is a function of V, X, D and F.

In figure 2, we show a graph (called a “Scoop” plot) showing apparent wavelength for a reflector at a specific depth and velocity as a function of offset and frequency. The yellow line shows the response if we also fix the frequency at 85 Hz. This shows that wavelength diminishes as offset increases. The pink line shows the response if we fix the offset at 1500 meters. This shows that wavelength diminishes as frequency increases. We can also demonstrate that wavelength diminishes as reflector depth decreases and as RMS velocity decreases.

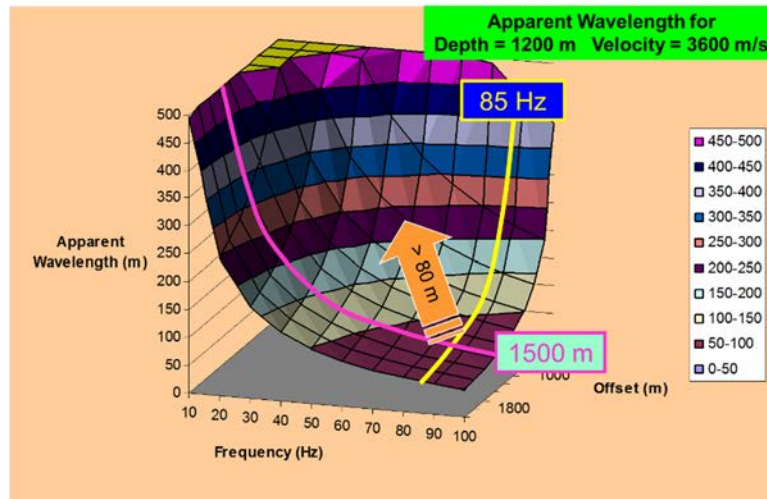


Figure 2. A “Scoop” plot where we have fixed the depth and velocity to a particular reflector and graph the apparent wavelength of reflections as a function of offset and frequency.

For any reflector, we expect apparent wavelengths of useable signal to range from infinity (at near offsets and low frequencies) downward to shorter wavelengths. The shortest apparent wavelength will be observed at the highest useable frequency and longest useable offset. These are values that must be estimated for each reflector of interest.

The highest useable frequency (F_{max}) is limited by earth absorption and noise floor. It decreases with depth of reflector and limits of dynamic range of the recording system (electronic noise). F_{max} also decreases with increased noise levels due to other modes of noise, but in this simple example we will not consider the noise (we assume the noise level is very small).

The maximum useable offset (X_{max}) can be limited by normal move-out stretch mutes, first break mutes or loss of energy due to long travel paths. As a general guideline, X_{max} can be related to depth of target and often lies in the range $0.8 D < X_{max} < 1.2 D$.

In the example in figure 2, we suggest for the modelled reflector at a depth of 1200 m with an RMS velocity of 3600 m/s, that F_{max} may be 85 Hz and X_{max} may be 1500 meters. In this case, reflections from this target will consist of apparent wavelengths ranging from infinity down to 80 meters. Considering all offsets from 0 to 1500 meters and all frequency contributions from 0 to 85 Hz, more than 40 percent of reflection signal components will consist of apparent wavelengths in excess of 500 meters. Only 16 percent of those components will have apparent wavelengths less than 150 meters.

In our design process, we run this type of analysis on several target zones from shallow to deep for each prospect. We have demonstrated that simple reflection signals emerge against the recording surface as long wavelengths. For reflections deeper than 1 second (two way travel time), apparent wavelengths are almost always longer than 80 meters. Some very shallow reflections (such as Canada’s heavy oil areas where targets are as shallow as 200 ms), exhibit emergent signals as short as 20 meters.

When designing seismic acquisition programs, it is important to consider the spatial sample interval required to measure all important events. Nyquist sampling theorem suggests that the separation between discrete measurement points should be smaller than one half of one cycle. For broad-band reflections, this means that the separation between observation points along a surface should be less than one half of the shortest apparent wavelength of desired signal.

In this simple model, we think the shortest wavelength to measure accurately may be 80 meters. Therefore a point receiver located every 40 meters along the surface (receiver interval) should be sufficient to preserve all elements of signal of interest to us. According to Nyquist, if we use a larger receiver interval, then the shorter wavelengths of desired signal will “alias”. That means they will appear in our data as if they were longer wavelengths and will contaminate our ability to properly measure the effected bandwidth.

Figure 3 shows the expected distribution of apparent wavelengths for the reflection in our example (1200 meter depth and 3600 m/s RMS velocity). The vertical scale is the relative abundance of frequency-offset components and the horizontal scale is the apparent wavelength of each component. Note that most software displays wavenumber on a linear horizontal scale. Wavelength is the inverse of wavenumber and we also display wavelength in our graphs as the dominant horizontal scale hi-lighted in pale yellow. Note that wavelengths decrease to the right and the scale is not linear.

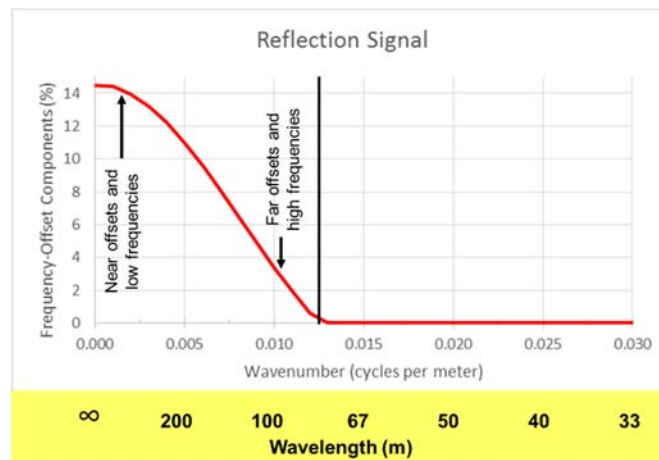


Figure 3. This distribution graph shows the relative abundance of reflection signal components for the reflection depicted in figure 2.

For a point receiver interval of 40 meters, the Nyquist wavenumber would be $1/(2 \Delta x)$ or 0.0125 m^{-1} or a wavelength of 80 meters (i.e. the Nyquist wavelength is just two times the spatial sample interval). This is represented by the vertical black line in figure 3. Signals with wavelengths from infinity down to 80 meters lie to the left of this line and will be measured correctly using a 40-meter receiver interval. Signals with wavelengths less than 80 meters (to the right of the black line) will not be measured correctly using a 40-meter receiver interval.

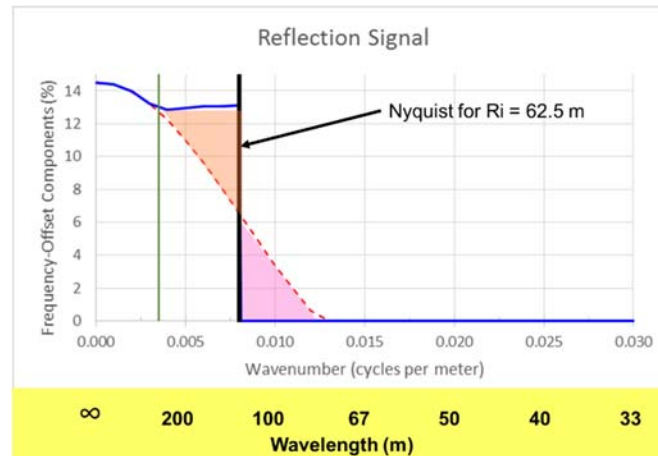


Figure 4. This distribution graph shows the effect of using a spatial sample interval that is too large.

However if we use a point receiver interval of 62.5 meters, then the Nyquist wave number will be 0.008 and the Nyquist wavelength will be 125 meters. Now we get the graph in figure 4. The dashed red curve shows the distribution of wavelengths along the continuous ground surface (the same as the solid red curve in figure 3). However, when we discretely measure with a spatial sample interval that is too large, two bad things occur.

First, we will fail to record any components that consist of wavelengths shorter than the Nyquist limit (the portion of the dashed red curve to the right of the vertical black line, shaded pink). Secondly, those components that lie to wavelengths shorter than the Nyquist limit will “wrap around” and will contaminate the true signal components immediately to the left of the Nyquist limit (the area shaded orange). The aliased amplitudes of higher wavenumbers (shorter wavelengths) will contaminate our estimates of the wavenumbers lower than the Nyquist (longer wavelengths). The contaminated wavelengths represent the higher frequencies and longer offsets of each shot record.

The resulting amplitude spectrum is represented by the solid blue curve. It accurately represents the emerging seismic signal only in the wavelength components to the left of the thin green line at a wavelength of 286 meters.

It is well known that when we discretely measure information, we must ensure that the sample interval is suitable for the details that we think are important to measure. No competent designer of 3D seismic programs will propose source or receiver intervals that are large compared to one half of the anticipated shortest wavelength of important signals.

Conclusions: Provided the surface of the earth where we record our receivers exhibits relatively long apparent wavelengths due to simple reflections of interest, then point receivers with a spatial sample interval smaller than one half the shortest expected wavelength will properly measure our desired signal. Smaller sample spacing is not necessary whether that would be provided by a distribution of geophones in an array or by a higher density of single point receivers. In figure 3, there are no contributing components with wavelengths shorter than 80 meters and a point receiver interval of 40 meters or less will be sufficient to provide accurate measurements of the emerging wave-field.

Deficiencies of Simple Model: This model considers only compressional wave components. Some geophysicists are interested in converted wave studies using down-going compressional waves and up-going shear waves. In P-S studies the conversion points are significantly different than P-P mid-points, emergent angles and frequencies are very different and RMS velocities are dramatically different. P-S studies generally require different spatial sampling compared with P-P studies (usually shorter intervals are required).

This model assumes homogenous materials between the surface and the reflector. More often we see layers of geology that represent a general increase in RMS velocity with depth. The result can be approximated by a “curved ray” model as opposed to this straight-ray approximation. Curved rays result in smaller angles of emergence of the wave-front against the recording surface and therefore result in longer apparent wavelengths. This would allow the use of larger spatial sample intervals.

This model assumes a flat and regular recording surface. If the surface where the receivers are located has a significant topographic slope, then the angle (α) in figure 1 should be increased or decreased by the angle of the slope depending from which direction the reflection arrives. This will either shorten or lengthen the apparent wavelengths depending on the direction of the slope relative to the source.

This model allows us to consider the range of wavelengths for individual reflectors. We must consider all reflectors of interest (including shallow zones where higher frequencies may allow improved statics solutions during processing).

This model considers only simple reflections. It does not consider more complex events such as diffractions. In our courses and design reports, we demonstrate that the maximum expected angle of emergence of diffractions within realistic useable offsets is about 35 degrees. We use that as a value for “ α ” when considering potentially productive targets.

This model does not account for any types of noise. In the next section of these notes, we will discuss the various modes of noise and their associated apparent wavelengths. It is very poor design practice to consider only the accurate recording of reflection signals. Inadequate measurement of some noise modes can render a seismic program virtually useless in some cases.

Noise Modes and Characteristics

The subject of various modes of noise that can occur in seismic data remains one of the most poorly understood aspects of our science. In this section, we will briefly describe some specific sources of noise and their characteristics.

1. Random Noise

Random noise generally refers to noise that is present in an area whether we are activating seismic sources or not. If it is truly random, then it contains all frequency components and therefore we sometimes refer to it as “white noise”. It is time-variant and unpredictable. However, the amplitudes of this noise are Gaussian distributed. That means that the average and standard deviation of the amplitudes remain about the same over time. Random noise does not contain bursts of high amplitude spikes or events.

There are very few real sources of noise that are truly random. The most common approximation to random noise in seismic data is perhaps noise due to wind and the wind moving sand or grass or other vegetation in the vicinity of our receivers. For geophone spacing larger than a couple of meters, we assume the wind noise is different on each receiver. If the noise is truly independent each time it is observed and at each different spatial location, then we may be able to improve the ratio of signal amplitude to random noise but averaging two or more traces that have been recorded with the same signal. We can apply the commonly quoted equation:

$$\text{Signal to Noise improvement} = \sqrt{N}$$

where N is the number of repeated traces. This can be the number of traces in a CDP gather (after NMO and statics corrections), or it can be the number of vibrator sweeps that are repeated at one source point, or it can be the number of geophones in an array whose outputs are averaged to produce one recorded trace. These are respectively referred to as CDP stack, Vertical stack and In-Group stack. The

signal to noise improvement is expected since the signal should add constructively amongst the N traces but the noise varies from trace to trace and will add destructively. Note that if the noise does not vary within the traces to be averaged (i.e. the noise is the same on each contributing trace), then the noise sums constructively as well as the signal and there is no signal to noise improvement by averaging the traces.

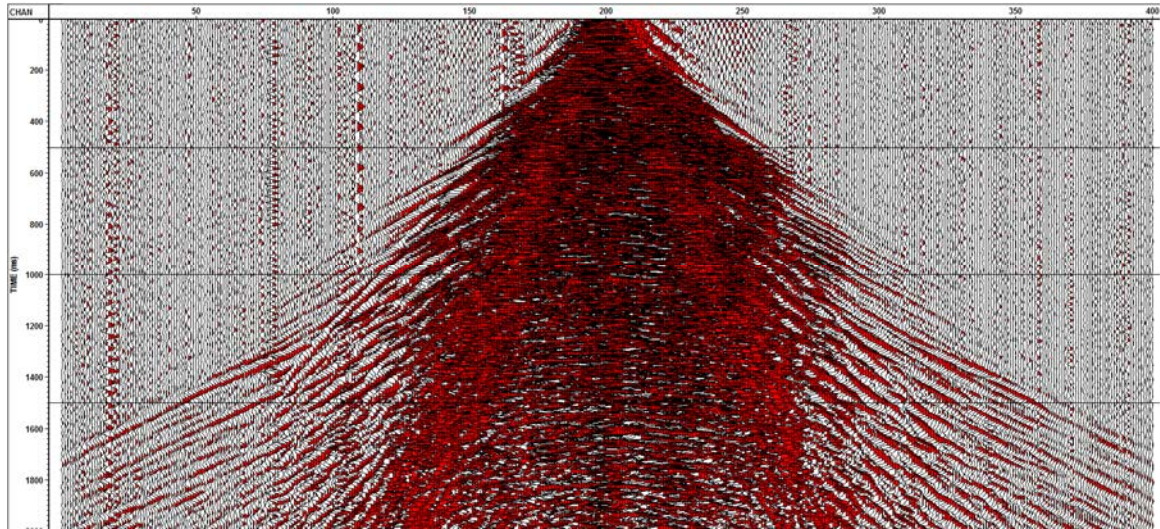


Figure 5. A fixed-gain display of a correlated vibroseis source record from a very windy area in Qatar.

Figure 5 shows a common source gather from a very windy area. This is a fixed-gain display of correlated vibroseis data. Note that at far offsets (the left and right extremes of the display), the receivers are reacting to some type of noise prior to the arrival of any source-generated waves. The noise is quite strong in amplitude, but still quite small compared to the source-generated surface waves and reflections.

Wind noise is typically measured in the range of a few micro-volts (less than 20) out of the pre-amplifier. Signals generated by a seismic source are often in the range of several milli-volts (more than 1000 times stronger (or 60 decibels). Although wind noise can occasionally hamper our seismic results, modern programs are generally high fold and wind noise is not considered a major obstacle.

Wind noise is usually controlled during field acquisition by suspending recording operations during periods of high wind. Random noise levels are monitored by measuring average output for each recording channel and comparing to contract standards. A better method involves comparing amplitudes of recorded “noise strips” to a high bandpass filtered fixed-gain display where key target reflectors are visible and ensuring that the noise levels are more than 12 dB weaker than the higher frequency components of important reflectors.

The use of distributed arrays of analog geophones may provide a superposition benefit (\sqrt{N}) provided the geophones are sufficiently separated so that each geophone observes independent noise but the same reflection signal as others in the array. In most projects, the trace generated by a distributed array of geophones has a somewhat better signal-to-noise ratio than a single point receiver in the same location.

Review of hundreds of vibrator sweep test programs has taught us that simple vertical stacking seldom provides any noticeable benefit to data. Therefore, we conclude that most projects do not have significant contributions due to random noise.

2. Erratic Noise

Erratic noise is not Gaussian distributed. The amplitudes can change significantly from one trace to another. The most common example is traffic and cultural noise. Engines and industrial activity can produce high amplitude noise on some traces but not on others. The time duration at any one location may be long-term (as in the case of a factory adjacent to a particular group of receivers), or it may last only a few seconds (as in the case of a passing vehicle).

The nature of the noise may be fairly random or it may be periodic (as in a generator or pump-jack operating near receivers). Erratic noise is not correlatable with the energy source. Its amplitude and phase is not predictable.

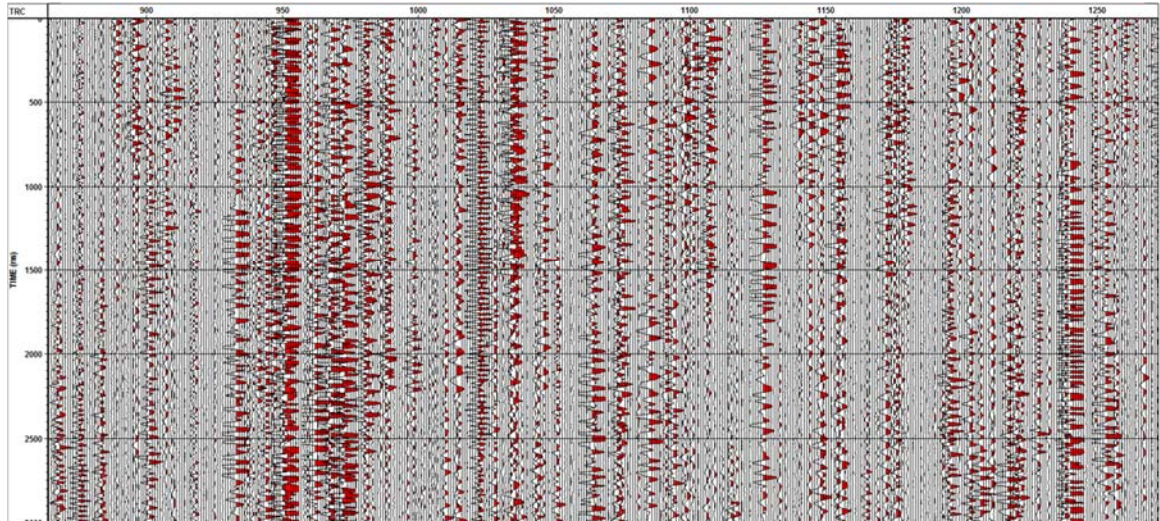


Figure 6. A fixed-gain display of a noise strip showing typical erratic noise near a town in Romania.

CDP stacking is not very effective against erratic noise since it is not sub-surface consistent. In areas of high cultural noise, there is little that can be done to eliminate erratic noise. Vibroseis correlation can be a fairly powerful tool. If the erratic noise varies in amplitude over a few seconds, then longer vibroseis sweeps are often more effective than shorter sweeps. If the erratic noise occurs in relatively short time bursts (a few hundred milliseconds), then diversity stacking of 2 to 4 sweeps per VP can be effective.

In figure 7, we show typical erratic noise, but we have added some synthetic reflection pulses every 200 ms. The amplitudes of the reflection pulses decrease by 6 dB with each successive pulse. We then compare a 2-fold normal average stack with a 2-fold diversity stack of the same data. Notice the very poor signal-to-noise ratio in the top display of figure 7 (normal stack) as compared to significantly improved signal-to-noise ratio in the lower display (diversity stack).

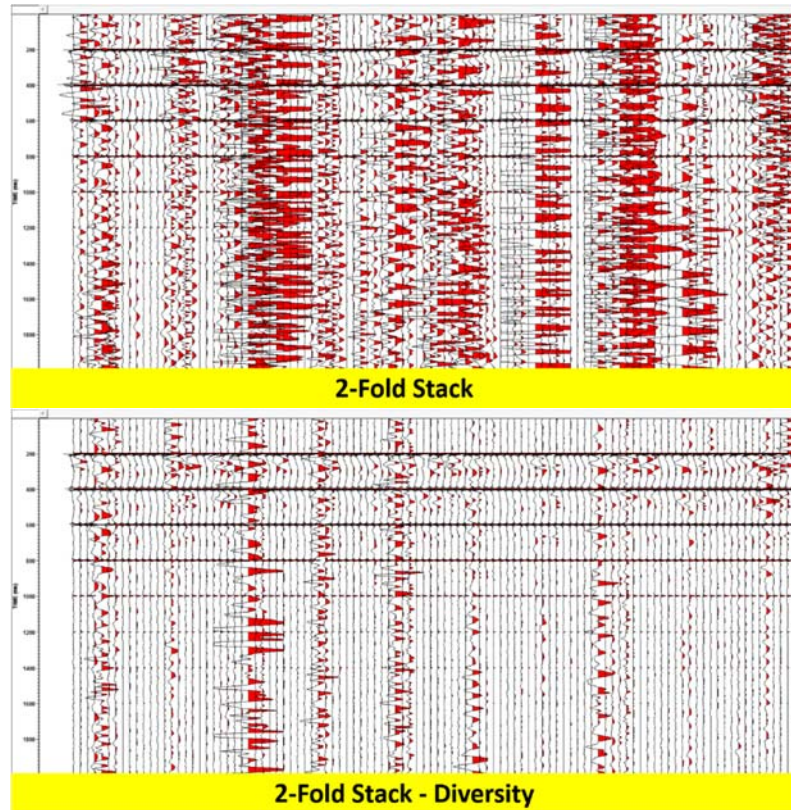


Figure 7. Erratic noise with synthetic reflectors added. Top display shows conventional 2-fold stack. Bottom display shows 2-fold diversity stack.

In data processing, erratic noise is somewhat mitigated by the careful application of F-X filter methods or Robust Cadzow filtering.

3. Noise Due to Irregular Source Behavior

Whether we use dynamite or vibroseis, our sources sometimes produce unexpected results. Fortunately, these artifacts are quite rare and generally not persistent over an entire program.

The image in figure 8 shows a dynamite record from the MacKenzie Delta of northern Canada. While drilling some of the shot holes, the drillers experienced high-pressure blowouts due to pockets of methane trapped in the frozen near-surface deltaic sediments. When these shot holes were detonated, the pockets of methane near the shot hole subsequently exploded and caused repetitions of the first breaks at unpredictable times. Vibrator source points recorded at the same location did not produce these artifacts. Although the dynamite artifact occurred in only a small percentage of the shot holes, it was very destructive to those shot records. This noise problem was solved by selection of vibroseis as the energy source.

Figure 9 shows a vibroseis record from a project in the foothills of the Rocky Mountains where truck-mount vibrators were used in hilly terrain. The reaction mass on truck-mount vibrators is positioned high within the stilt structure in order to provide space to pass the drive-shaft of the power train. This creates a less stable structure when the unit is not on flat ground and emphasizes rocking harmonics. The ringing pattern below two seconds on this record parallels the first breaks and is a result of low-order harmonic distortion correlating with fundamental frequencies in positive time during correlation. Truck-mount vibrators are a poor choice of energy source when terrain is not flat.

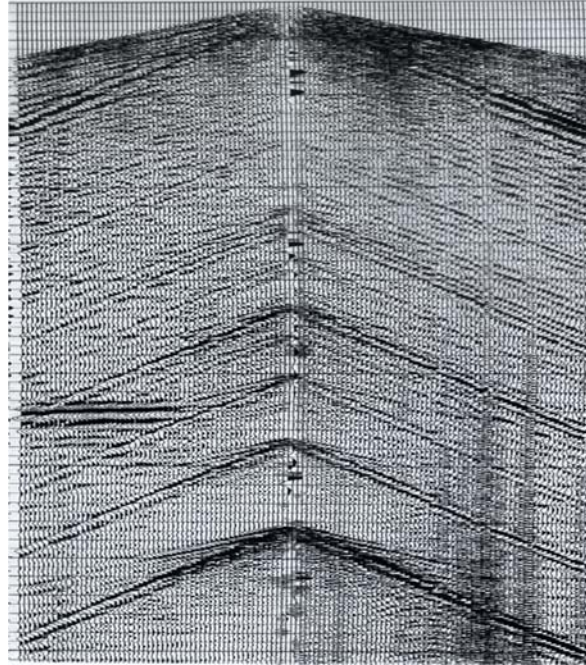


Figure 8. This dynamite record was recorded in the MacKenzie Delta. The initial detonation was fired at time zero, but pockets of methane in the immediate vicinity of the shot hole resulted in secondary detonations as evidenced by later copies of the first breaks. This display shows 3.5 seconds of data, 120 channels at 30 meter intervals.

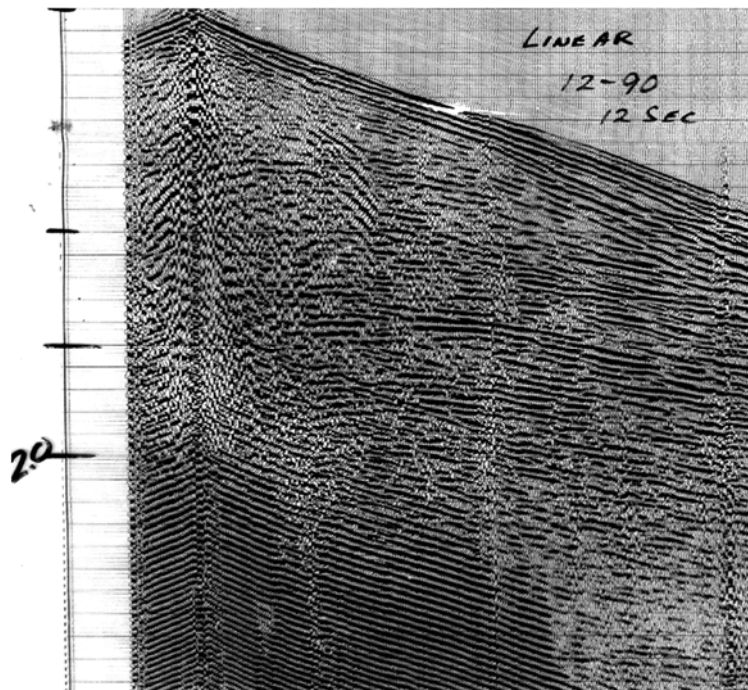


Figure 9. This correlated vibroseis record was recorded in hilly terrain in Northeast British Columbia using truck-mount vibrators.

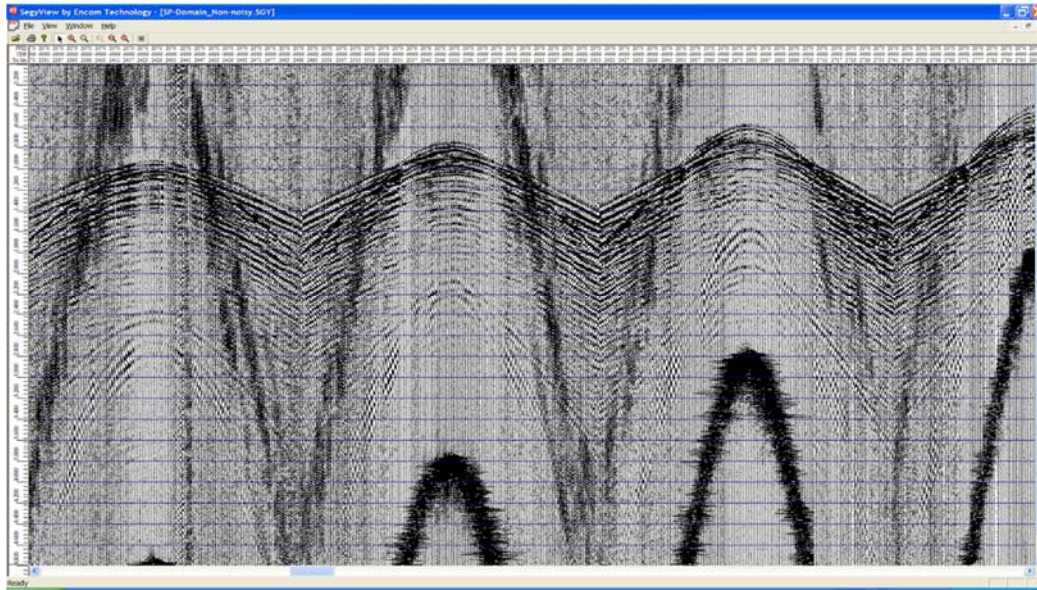


Figure 10. This correlated vibroseis record was recorded in the Western Desert of Egypt.

Figure 10 is an example of a very high amplitude high-order harmonic correlating in negative time with the fundamental sweep. This was due to a unique combination of abnormally strong correlated air wave and an abnormally strong third harmonic. That harmonic came from a pulse-like behavior when the reaction mass dropped abruptly at earth resonance and the sand evacuated from below the base plate due to liquefaction.

We must choose our seismic equipment prudently and be aware of potential liabilities in different environments.

4. Coherent Source-Generated Noise

Coherent events are peaks or troughs that seem to line up along a straight line or predictable curve from trace to trace. Sometimes, coherent events appear on our data whether we activate a source point or not. These would NOT be considered source-generated noise. They may result from dynamite shots from other nearby seismic programs, earthquake events, induction from power lines, generators near our line, some types of heavy and slow traffic, et cetera. These types of noise will appear on common source gathers and also on wind strips. Many are not avoidable, and some are avoidable by re-locating the receiver lines. We will not address coherent non-source-generated noise in this dissertation as the potential for remedies have to be considered on a case-by-case basis. Usually only a few shots or a few receiver groups are affected and often only at occasional times. These problems do not accumulate in the subsurface and reasonably high-fold designs are often a sufficient mitigation.

Here we are defining noise as any events that do not help us image our geologic targets. Note that reflections are generally coherent from trace to trace and are generated by activating our source, but we refer to those as signals. Diffractions are also coherent, but follow different move-out trajectories compared to reflections. Diffraction patterns may not be viewed as an image of a geologic layer, but migration of diffractions certainly contributes to clear images of geology.

Multiples will also produce coherent events on raw data. Some multiples can be modelled and may contribute to the imaging of primary reflections. Otherwise we tend to rely on various processing algorithms to suppress multiples. In this paper, we will not treat multiples as a noise mode to be dealt with in design or acquisition other than sufficient offsets must be recorded to give the processor some leverage to suppress them.

All seismic records will contain at least one of several forms of coherent source-generated noise. Figure 11 is a display of a simple 2-layer (three boundary) model using flat layers and homogeneous and isotropic materials in each layer. We recorded the vertical component of ground velocity for receivers located every 2 meters along a flat surface. Notice that vertical component does NOT mean P-wave. Single component sensors are not P-wave sensors, they are vertical motion sensors. In fact, for horizontally propagating shear waves, the vertical component of ground motion is much stronger than the vertical component of horizontally propagating compressional waves.

The source was simulated by an omni-directional, minimum phase pulse. Source generated surface waves include the direct P-wave and refracted P-wave (compressional waves) which together constitute what are commonly called “First Breaks”. Measurements of these events assist in developing the near-surface low velocity layer and weathering layer models that become an important part of statics solutions during processing. Other than that, surface waves do not contain information about the deeper reflectors of geologic interest.

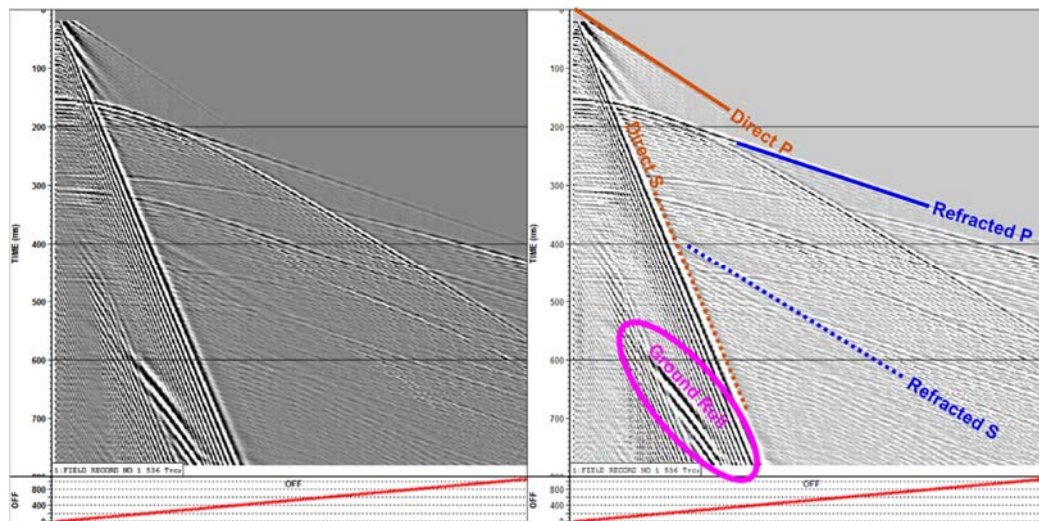


Figure 11. This record was generated using Tesseral Wave Equation Modelling.

Each of these surface waves also have a shear-wave equivalent that follows the same path but at a much slower velocity. These are indicated in figure 11 by the dashed orange and dashed blue lines. The shear-converted direct wave (direct S) is often incorrectly labelled by many geophysicists as “Ground Roll”. Note that the shear-converted direct wave reverberates strongly. This is due to the trapped mode behavior that normally results from low velocity poorly lithified materials overlying a high velocity lithified rock boundary (bedrock)

Ground roll is a complex elliptical retrograde wave that travels slowly away from the energy source. It consists of alternating shear and compressional behavior. This causes it to be dispersive. It can be represented by a “group” velocity (the speed of propagation of the wavelet package) and a “phase” velocity. The phase velocity is the apparent alignment of the peaks and troughs. When it is properly sampled it appears somewhat like overlapping shingles on a roof. This is because the mode of the propagating wave (and therefore its apparent phase) is alternating from shear to compressional behavior twice each cycle. The apparent wavelength of most components of ground roll is very long and mostly overlaps the wavelength bandwidth of desired signal. To filter ground roll with a spatial filter (K-domain filter) would also filter significant signal bandwidth and would be destructive to desired data.

Note that the shear-converted direct wave forms a limit to the appearance of ground roll. It has been demonstrated that the fastest group velocity of ground roll cannot exceed the shear-wave velocity of the near-surface material.

In the early 1990's John Tessman and others experimented with adaptive filters to eliminate ground roll using the digital 3-component VectorSeis sensors that were released around that time. By recognizing the unique oscillation of ground roll between horizontal and vertical particle motion, it could be separated by adaptive filtering. This did not gain much popularity, partly because it only attacked the true ground roll and did not attack the shear-converted direct wave (which stays in a constant phase as it propagates). Since most people consider the shear direct wave to be ground roll, it was perceived that the filter was not very effective.

Ground roll exists only about a half to one wavelength into the subsurface. Since lower frequency components of ground roll reach deeper into the sub-surface, their group velocity is generally faster than higher frequency components (which only penetrate a very shallow part of the near surface). This is due to the fact that most near-surface materials increase in velocity due to depth of burial and consolidation. This results in a velocity dispersion that can be measured and attributed to the near-surface velocity model. Some geophysicists are using inversion of ground roll to create models of the near surface that are sometimes better than conventional refraction or tomographic methods.

Figure 12 shows the same events as described for figure 11, but using real data. In figure 12, we can measure the velocity of the direct and refracted compressional (P) waves as 2080 m/s and 2810 m/s respectively. We can also measure an intercept time for the refracted wave at 28 ms. Using a conventional 1 layer flat LVL model, we would calculate the depth to the refracting boundary as 43 meters.

We can also measure the velocity of the converted shear direct and refracted waves as 960 m/s and 1250 m/s respectively. We can then estimate the V_p/V_s ratio for the LVL layer at 2.17 and for the refracting layer at 2.24. These are fairly typical for lithified sediments. Very often the LVL layer is poorly lithified and it is common to see V_p/V_s ratios of 3 or 4.

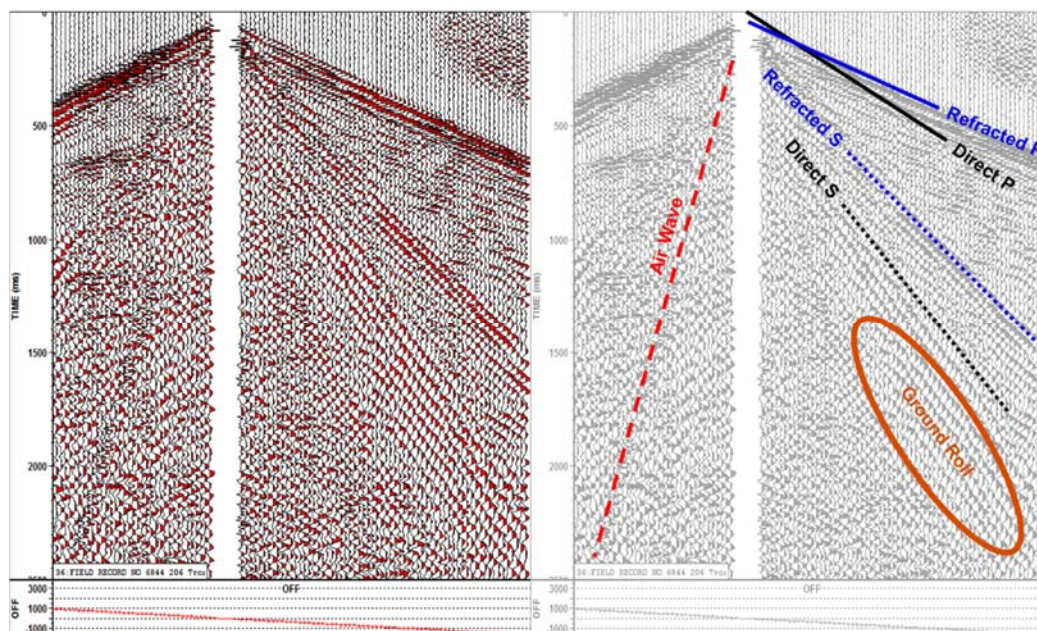


Figure 12. Correlated vibroseis record from Mexico showing some surface waves in real data.

We can also see the correlated air wave. In this case its velocity is 360 m/s. The data was recorded near sea level on a humid day, so the velocity of sound in air was a bit higher than usual. The normal range is about 300 to 340 m/s. The correlated air wave will be broadband (with all the frequencies of the sweep used) and presents as a short-duration wavelet propagating at a predictable velocity. It does not present any significant problem in processing.

The slow surface waves are high amplitude as they have very short travel paths compared to deep reflections and they do not experience transmission losses across reflective boundaries. When they span a broad range of velocities and if they reverberate significantly, they can be quite destructive to data quality. However, they generally lie only in fairly predictable zones of the source record. Provided their velocities are quite slow, they can usually be suppressed with robust linear noise removal algorithms.

The fast surface waves (first breaks) are used for refraction analysis and help provide near-surface velocity models for statics solutions. Once this information is obtained, the high-energy first breaks are usually eliminated by muting. This also is one of the factors that may impose a limit on maximum useable offsets where the linear first break mute intersects reflection hyperbolae from reflectors of interest.

If the base of the low velocity layer forms a very strong reflection coefficient, this will usually result in strong reverberations of the surface waves. These are referred to as “trapped mode” or “guided waves”. Figure 13 shows two examples of strong trapped mode reverberations. If the thickness and velocity of the near-surface layer is quite uniform, the guided wave will be monochromatic with a frequency $F = V/2D$ (where V is the velocity of the low velocity layer and D is the thickness to the highly reflective boundary at the base of the layer). In this case, the LVL velocity is about 1700 m/s and the depth to bedrock is about 60 meters, yielding a guided wave frequency of about 14 Hz. This is equivalent to one wavelength over the two-way travel distance through the guiding layer, which becomes the sustained signal. The right hand record also shows the second harmonic of the guided wave where two wavelengths are sustained.

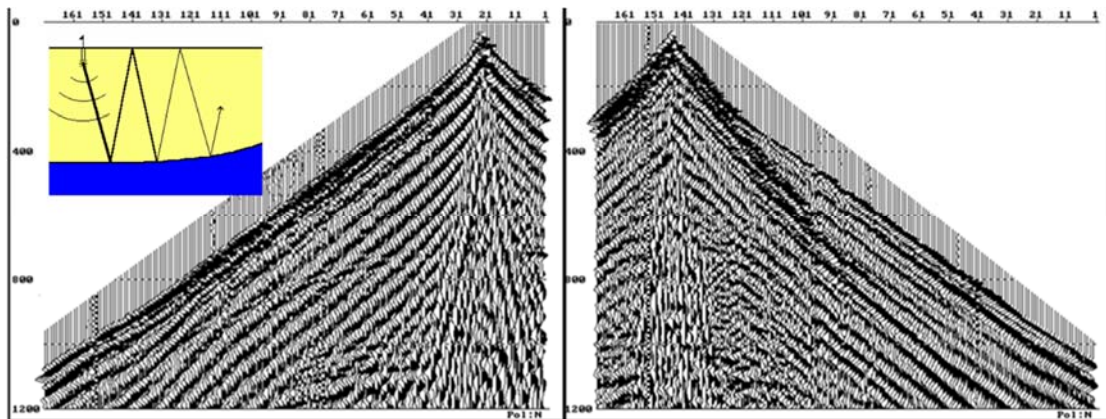


Figure 13. Examples of strong trapped mode from Gordondale area in Alberta.

One indication of whether or not to expect strong trapped mode noise is to examine the first breaks. Notice on the record on the right of figure 13 that the direct wave is very slow (steeply inclined) and the refracted wave is quite fast (somewhat flatter). This forms a pronounced wedge shape between the two. If that wedge is very obvious, this means there is a great difference between the velocity of the low velocity layer and the velocity of the underlying refractor and we will be vulnerable to trapped mode.

In this case, the LVL is 1700 m/s and the refractor is 3000 m/s. In figure 14, we demonstrate a source that emits energy in all directions below the surface. The source energy spreads out in a hemisphere. But when that wave-front encounters the boundary at the base of the LVL, it experiences refraction. Portions of the wave-front that encounter the hard boundary at the critical angle or less will bifurcate and some energy will transmit to deeper layers and some will reflect back towards the surface. But any part of the hemispherical wave-front that encounters the boundary at an angle greater than the critical angle will be 100% reflected with no transmission into deeper layers.

The portion of the surface area of a hemisphere that intersects a plane within a cone described by the critical angle is $1 - \cos(\alpha)$ where α is the critical angle (or $\sin^{-1}(V1/V2)$). For this example, that means that only about 18 percent of the generated source energy will be available to transmit through the hard boundary at the base of the LVL. However, within the area of that critical cone, some of the incident energy will also be reflected. The reflection coefficient at vertical incidence will be about 28 percent, but the average reflection across the area within the critical cone will be more like 34 percent. Therefore, only about 66 percent of the energy within the critical cone will pass the base of LVL and only 18 percent of the source-generated energy will lie within the critical cone.

Therefore, about 12 percent of our generated source energy will pass the base of LVL to continue downward and generate reflections while 88 percent will remain trapped in the low velocity layer (assuming that almost all upward going energy is nearly 100% reflected back down by the free-air boundary). The limited energy penetration means reflection signals from deeper geology will be weak and the large amount of energy trapped near the surface means that the source-generated surface waves will be strong. In this case, the potential signal due to transmitted energy will be about 18 dB weaker than the potential noise generated by the trapped mode.

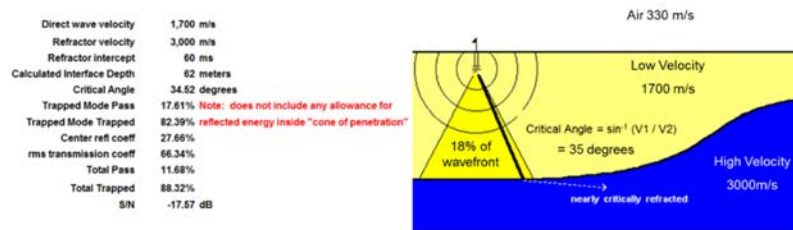


Figure 14. Determining potential for trapped mode based on first break velocities.

In fact, in figure 13, we can see some evidence of hyperbolic reflections amidst all of the reverberating noise trains. If that noise is only 12 to 18 dB below the level of the linear noise trains, this can be easily solved with processing. The noise is dominantly mono-chromatic and quite uniform in velocity. Even a simple spiking deconvolution is quite successful at lifting the broadband signal from below the monochromatic noise. Although the noise looks very scary on the raw data records, it is not too serious a problem and can often be managed in processing.

Figure 15 shows the results of wave-equation modelling of a very simple geologic model. The X-Z model on the left shows a flat surface extending 3000 meters from a shot point at the left end. There is a single homogeneous and isotropic layer 1600 meters thick with a compressional wave velocity of 2800 meters per second. There is a flat boundary with the next layer, which has a velocity of 3500 meter per second.

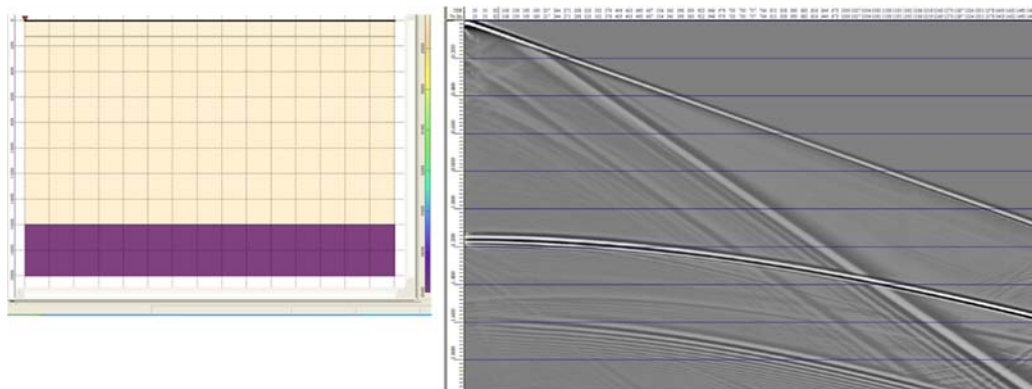


Figure 15. A very simple geologic model with the wave-equation modelled X-T record.

On the right of figure 15, we show the vertical component of ground motion using a receiver interval of 2 meters from 0 to 3000 meters offset (the X-T display). We see a clear high-frequency linear event representing the direct P-wave travelling from about 0 to 1100 ms across the record. We also see another weaker and lower frequency event due to the direct S-wave travelling from about 0 to 2000 ms across the record. The two most obvious hyperbolic reflectors have zero-offset arrival times of about 1180 ms and 1600 ms. They represent the P-P reflection and the P-S reflection respectively. Most of the other very weak events are artifacts due to the model boundaries.

Figure 16 shows a slightly more realistic model. The X-Z model is similar to that in figure 15, but we have replaced the first 150 meters below the surface with a flat low-velocity layer with a compressional wave velocity of 1800 meters per second. This creates first breaks that consist of the direct P-wave and refracted P-wave. We get reflections and multiples from the shallow base of LVL boundary.

The amplitude of the deep P-P and P-S reflections are dramatically reduced due to limited transmission through the strong reflection coefficient and critical angle limitations similar to those depicted in figure 14 (in this case approximately 17 percent of the generated source energy will pass the base of LVL boundary). But we also see a significant amount of reverberation of the direct and refracted P-waves that result in a complicated pattern of noise that dominates the reflections at mid to far offsets. Note that much of this noise exhibits apparent wavelengths significantly shorter than the shortest wavelengths of the reflectors.

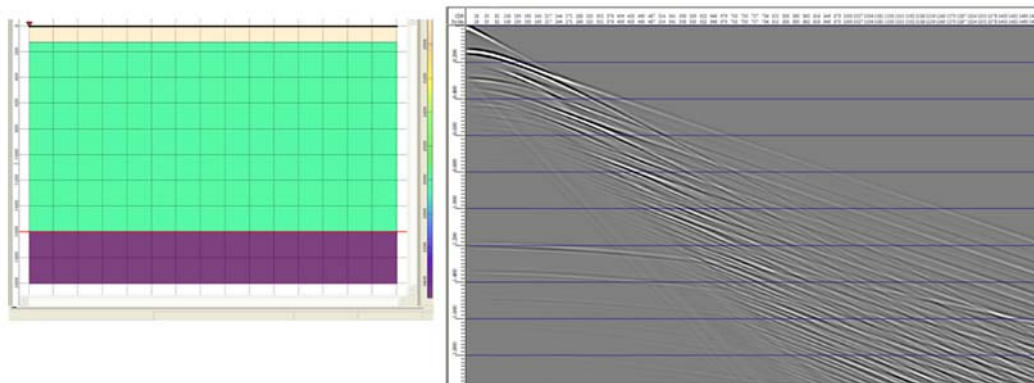


Figure 16. A slightly more complex geologic model with the modelled X-T record.

5. Chaotically Scattered Source-Generated Noise

The examples in the previous section illustrate noise that is coherent from trace to trace over fairly long distances. These are often referred to as “noise trains”. However, source-generated noise trains may not remain coherent in appearance due to a number of factors.

Figure 17 shows two correlated vibroseis records. They were both recorded from the same source point by the same receiver spread. They were recorded the same day, but about 20 minutes apart. Both used the same vibrators and the same sweep. The record on the left was from a single sweep. The record on the right is the average of 12 sweeps taken on the same pad positions.

There is some coherent reflection energy evident at a couple of levels below 600 ms. There is some coherent surface wave energy evident near the top of the record. However, much of the records appear to be dominated by random noise. In the highlighted red boxes, we see no evidence of any coherent events. But when we examine the traces in those highlighted areas very closely, we see the character of the noise is exactly repeated!

A noise strip recorded earlier in the day from these same receivers shows no evidence of these same wavelets. The noise on the wind strip from these channels measured less than 20 micro-volts in the raw data. The wavelets we see on the records in figure 17 measure several millivolts. The noise in the highlighted boxes is NOT wind noise or ambient background noise. If it was time-variant Gaussian-distributed noise, the signal to noise ratio would be improved by averaging 12 traces in the record on the right. But the two records are nearly identical!

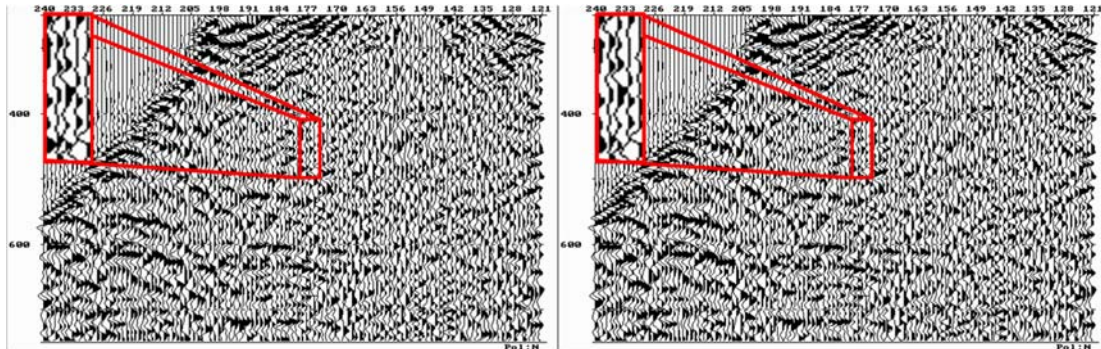


Figure 17. Correlated and summed records from near Colville Lake in the Northwest Territories of Canada

These wavelets of noise we see are not correlatable from trace to trace, but they are exactly repeatable for records made at different times from the same source point. They are not present on the receivers when we do not activate a source. This noise is obviously source-generated, but at this trace spacing it is certainly not coherent.

We have conducted vibroseis sweep tests on several hundred prospects in a broad variety of countries, geologic basins and geographic settings. One part of our suite of tests is always an effort test where we compare data using the average of 1, 2, 4, 9 and sometimes more sweeps using the same sweep at the same location. In more than 80 percent of our tests, we observe no significant difference in normalized records generated using more than one sweep per source point. We very seldom observe the \sqrt{N} signal to noise improvement predicted by theory that assumes noise is random.

Furthermore, any source that may generate useful reflections at desired geologic targets, will also create source-generated noise. Bigger source effort generates more signal but also generates more noise. The noise problem we see in figure 17 cannot be solved by changing source parameters. This problem occurs in all types of vibroseis data and also in dynamite data. Dr. Rodney Calvert of Shell once re-recorded data from an 18 year old 2D dynamite seismic line, replicating the parameters as accurately as he could. When he compared raw records from the original survey to records recorded 18 years later from the same location, he found the wavelets of noise to be exactly repeated. That included noise that had a random appearance and was originally attributed to “background” and “ambient” noise.

We refer to such noise as “chaotically-scattered source-generated noise”. So let’s examine some of the mechanisms that can cause such a phenomenon.

So let’s go back to the trapped-mode guided waves we showed in figure 13. But let’s consider what happens in any wave-guide if the velocity or thickness of the wave-guide changes abruptly. Recall that such a situation will result in reflection of the guided wave. This is demonstrated in figure 18 and a real-data example is shown in figure 19.

Figure 19 is a fascinating example of how abruptly noise due to surface conditions can change. This is a single shot record from a 2D line where the right side of the shot lies in the ancestral valley of a river and the left side of the shot is in undisturbed ancestral sediments. The photo at the top of the record shows the location of the shot record relative to the river.

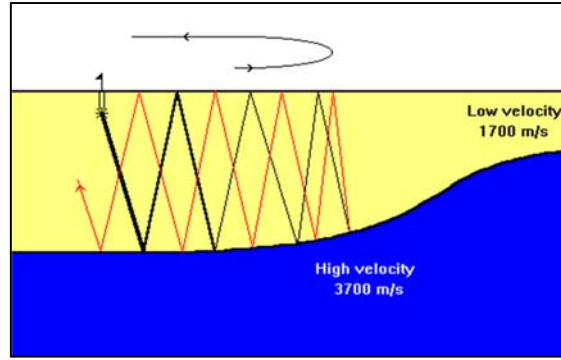


Figure 18. An abrupt change in velocity or thickness of a wave-guide will cause reflection of the guided wave.

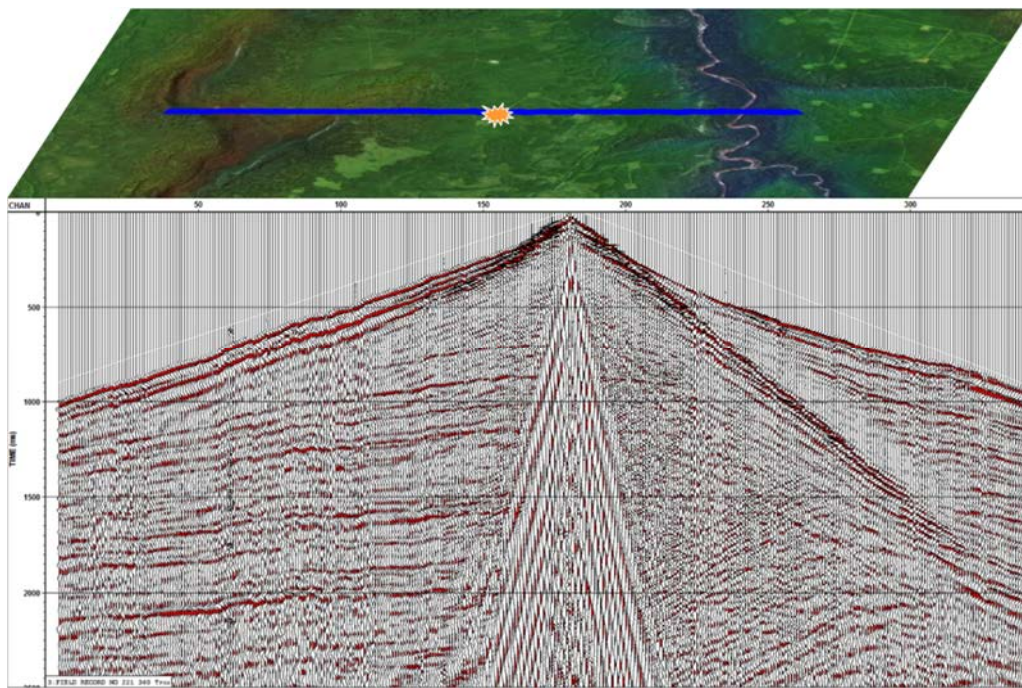


Figure 19. Back-scattered surface waves on one side of a shot record near a river in Northeast British Columbia.

Figure 20 presents two simple geologic cartoons that show how a present-day active river may have a very wide ancestral valley where it has meandered over the past several thousand years. The right side of this figure shows in concept the complicated distribution of various fluvial sediments that may lie within the ancestral valley. Sometimes, the most complex geology we encounter is in the near surface.

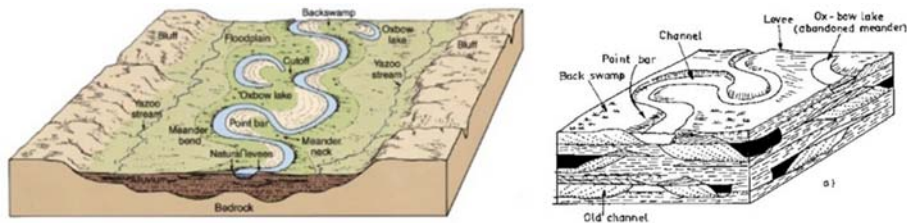


Figure 20. Geologic models showing an active river and its ancestral valley (left). On the right is a conceptual model of the complex features that may lie within the ancestral valley.

The left side of the shot record in figure 19 exhibits good data with many reflections from the subsurface. However, on the right side, the reflections are masked by a variety of noise modes. Most obviously, we see a strong, slow direct wave (1540 m/s) that persists across the entire right side spread. This is the direct wave as it exists across the fluvial sediments that fill the 70 to 100 meters of ancestral river valley. We also see the much faster refraction (2600 m/s) from the base of the fluvial sediments. This base of the ancestral valley is same material that exists regionally just below a thin weathering layer in the areas outside the ancestral valley. Note the large wedge between the refraction and the direct wave; this is a sure indicator or potential data problems. We also see reverberations of both direct and refracted waves (due to trapped mode behavior).

Extending downwards and to the left from the strong direct wave, we see other linear segments of coherency. These are back-scattered direct waves moving along the near-surface layer backwards towards the source location.

In addition to these coherent linear events, the data on the right side of the record has a generally high level of what many geophysicists would call random noise. However, when a source point is repeated from the same location, the details of this noise are exactly repeated. Therefore, it is another example of chaotically-scattered source-generated noise.

Figure 21 shows a Tesseral wave equation model of a shot acquired in an area where the near surface layer is homogeneous and isotropic. The shallow part of the model is shown at the top of the figure (the top 300 meters). The yellow layer has a compressional velocity of about 3000 meters per second. The generated shot record shows clear coherent linear events (surface waves) and clear and strong hyperbolic events (reflections from deeper layers in the input model).

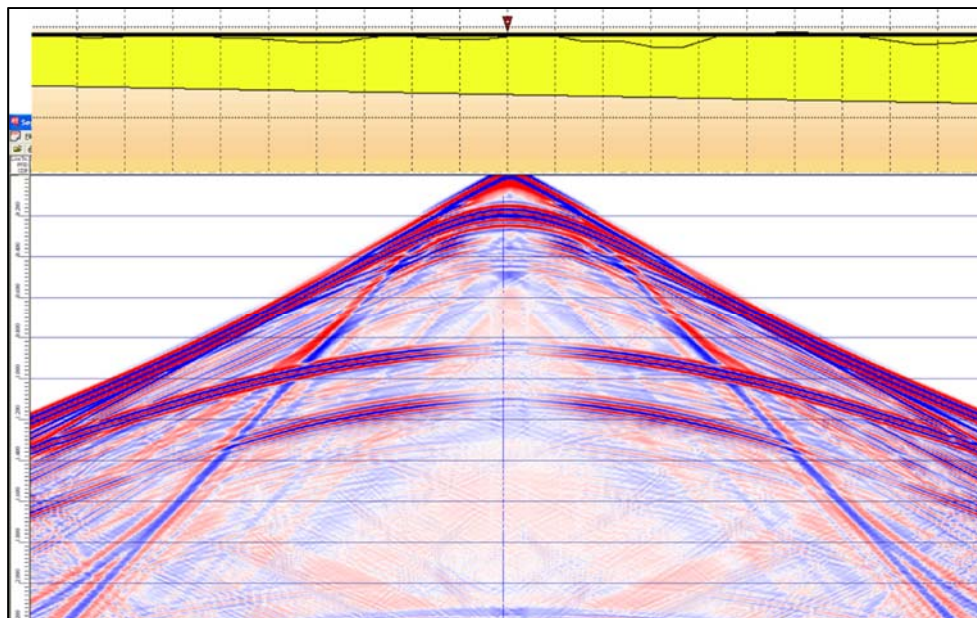


Figure 21. Tesseral wave equation model for a shot record in an area with a flat surface and homogeneous and isotropic near-surface layer (yellow layer in model at top of figure).

Figure 22 shows the same model but the near surface layer now includes a low velocity layer (1600 m/s) of variable thickness from a few meters to about 60 meters. The LVL is shown as a green layer replacing part of the yellow layer. The generated shot record shows reverberations associated with all of the linear surface waves. The hyperbolic reflections are much weaker due to the poor penetration of source energy through the base of the low velocity layer (review figure 14).

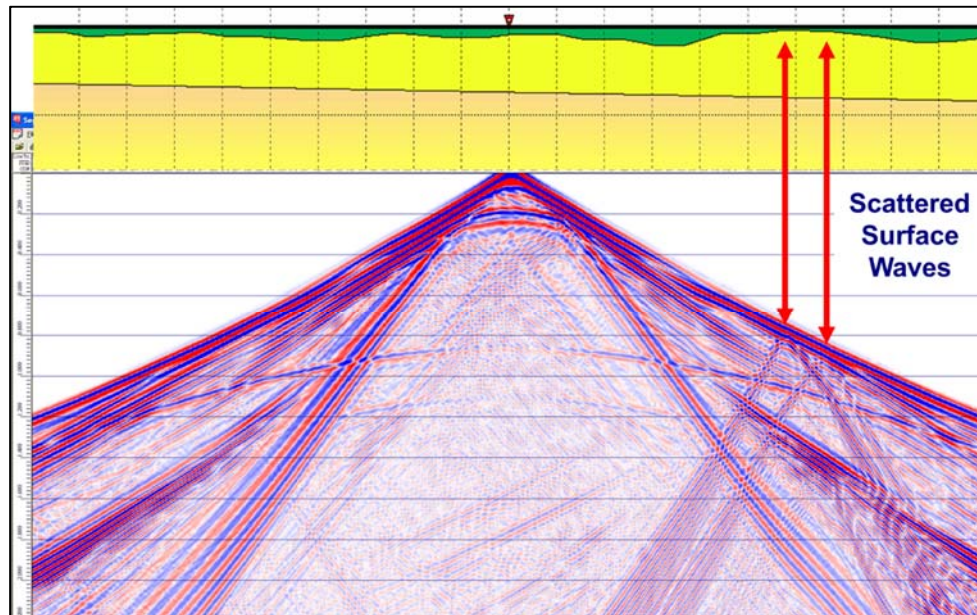


Figure 22. Tesserale wave equation model for a shot record in an area with a variable low velocity layer (green).

However, we also see some new events that appear like linear events generated by secondary shots at the locations indicated by the red arrows. If these were secondary shots they would have to have been initiated at the exact time that the first breaks from our primary shot arrived at those offsets. In fact, these are scattered source energy caused by the abrupt change in the material velocity in the near surface. Any such inhomogeneity in the near surface can cause such scattered events.

In figure 22, the scattered events appear linear because the inhomogeneity lies directly along the line of receivers. But what if the inhomogeneity lies to the side of the receiver line? In figure 23 we show a map of a 2D shot record obtained in Northeast British Columbia. The shot record is shown in figure 24. This line is also near a river (a tributary of the larger river shown in figure 19).

In figure 23 the blue symbols represent the locations of receivers that form the shot record and the red square near the center of the line of blue symbols is the location of the energy source. The solid yellow concentric circles represent the propagation of the direct wave across the surface at a velocity of 2040 m/s. The circles progress from a radius of 300 m (147 ms) to 850 m (417 ms), 1400 m (686 ms), 1950 m (956 ms), and 2500 m (1225 ms). The black symbol lies near a minor topographic escarpment that forms the edge of the ancestral valley of the river. We believe this point acts to scatter the surface waves. The solid red line shows the path of the direct wave from the source point to the black symbol, a distance of 1400 meters (686 ms – the third solid yellow circle). The black scattering point then creates another direct wave (it acts as a Huygens scattering point). The direct wave from that scattering point then propagates as described by the dashed yellow concentric circles. 539 ms later, the scattered direct wave arrives at the blue line of receivers, a total of 1225 ms after the shot was initiated. By this time the original direct wave from the shot point has propagated along the blue line to as far as the largest solid yellow circle.

The associated shot record that we see in figure 24 shows the direct wave propagating from the shot to the right at a velocity of 2040 m/s (green line). We also see a hyperbolic artifact with its apex indicated by the yellow arrow (at an offset of 830 meters and arrival time of 1225 ms). This is the first arrival of the scattered direct wave from the scattering point indicated by the black symbol in figure 23.

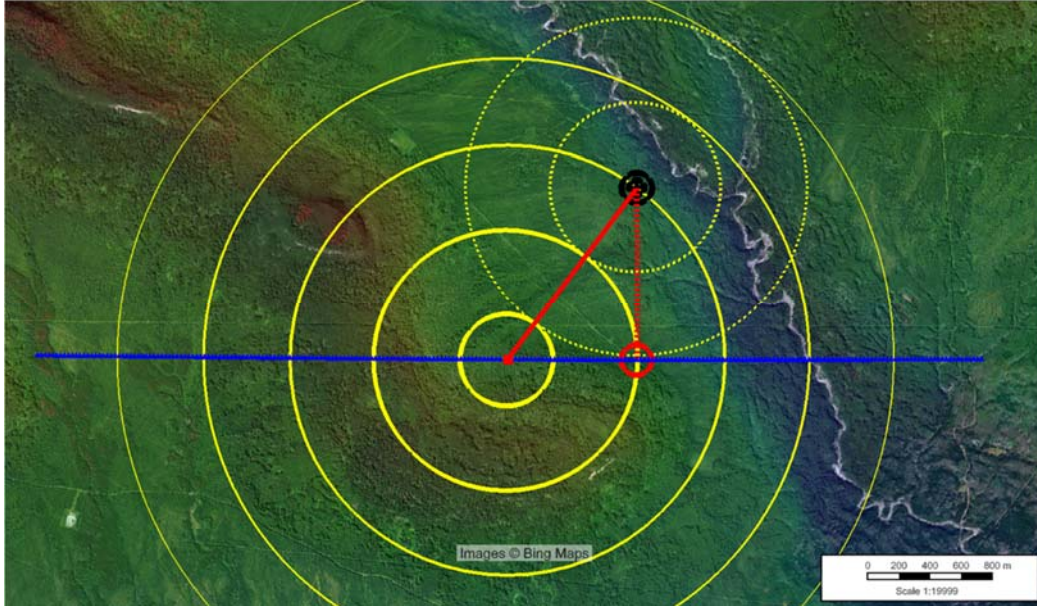


Figure 23. Map view showing the location of the shot record shown in figure 24. The yellow rings represent the propagation of the direct wave at times of 147 ms, 417 ms, 686 ms, 956 ms and 1225 ms. The solid red line shows the path from the source point to a scattering point at the edge of the ancestral valley of a river (black symbol). The dashed red line shows the path from the scattering point to the receiver line where it will be observed.

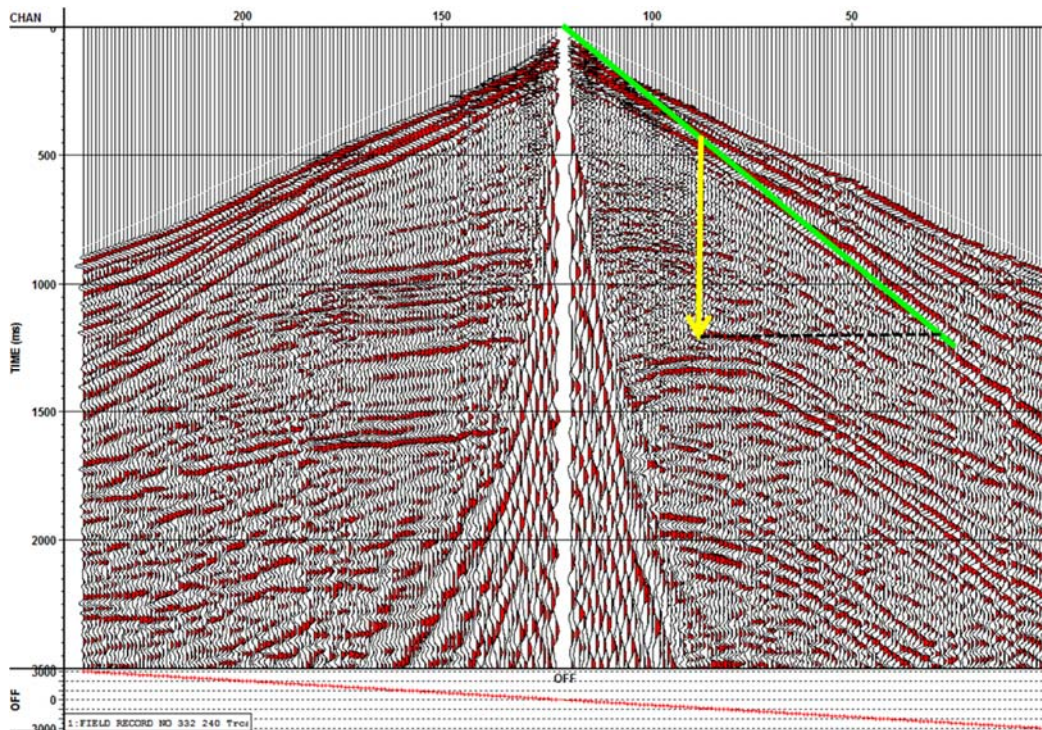


Figure 24. The shot record obtained from the image in figure 23.

At 1225 ms (indicated by the dashed horizontal black line in figure 24) the original direct wave generated by the shot point is arriving at a receiver 2500 meters away from the shot. At the same time, the direct wave has travelled from the shot to the scattering point and back to the receiver line at an offset of 830 meters (tip of the yellow arrow). The scattered direct wave appears hyperbolic below this point since the source of the wave is broadside to the line of receivers (not in-line).

A relatively simple scattered event such as this might be removed in processing by predictive modelling and subtraction. However that would require reasonably firm knowledge of the location of the scattering point and the near-surface velocities between the observation line and the scattering point. This information will seldom be known with sufficient confidence to justify predictive filtering.

The record in figure 24 is very rare in land seismic data as we very seldom see a single scattering point such as this. Figure 25 shows a more common occurrence with several hyperbolae due to various scattering points. Notice the prominent wedge between the slow direct wave (1750 m/s) and considerably faster refraction (2700 m/s). The receiver interval on this data was 10 meters, so it is quite well sampled spatially. We see strong reverberation of the refractions (guided waves) suggesting we are in an area with a fairly stable low velocity layer. The few occurrences of scattered waves on the left side of the record suggests we may be approaching an area that contains some scattering points. The time difference between the apex of any hyperbola and the direct wave immediately above that point is partly a function of the lateral offset of the scattering point relative to the receiver line.

The reflectors in figure 25 are quite clear and this data would be considered generally good. The processor should be able to perform velocity analysis and statics solutions and CDP stacking with reasonable fold should provide good seismic sections.

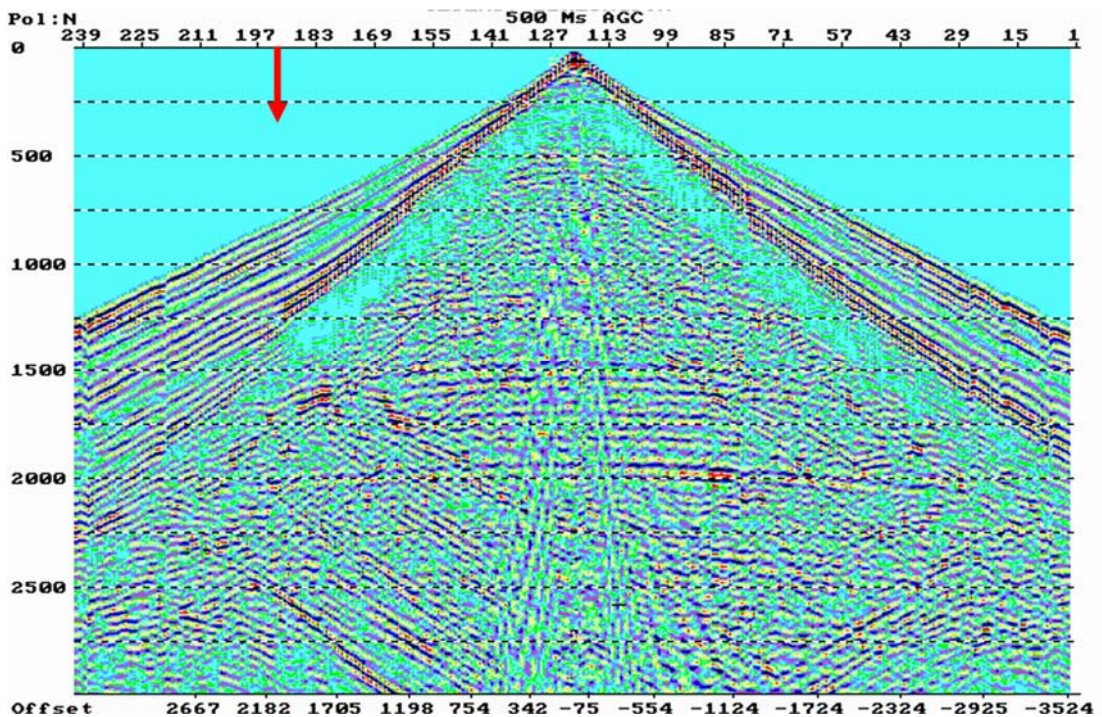


Figure 25. A more typical shot record showing several scattering point hyperbolae.

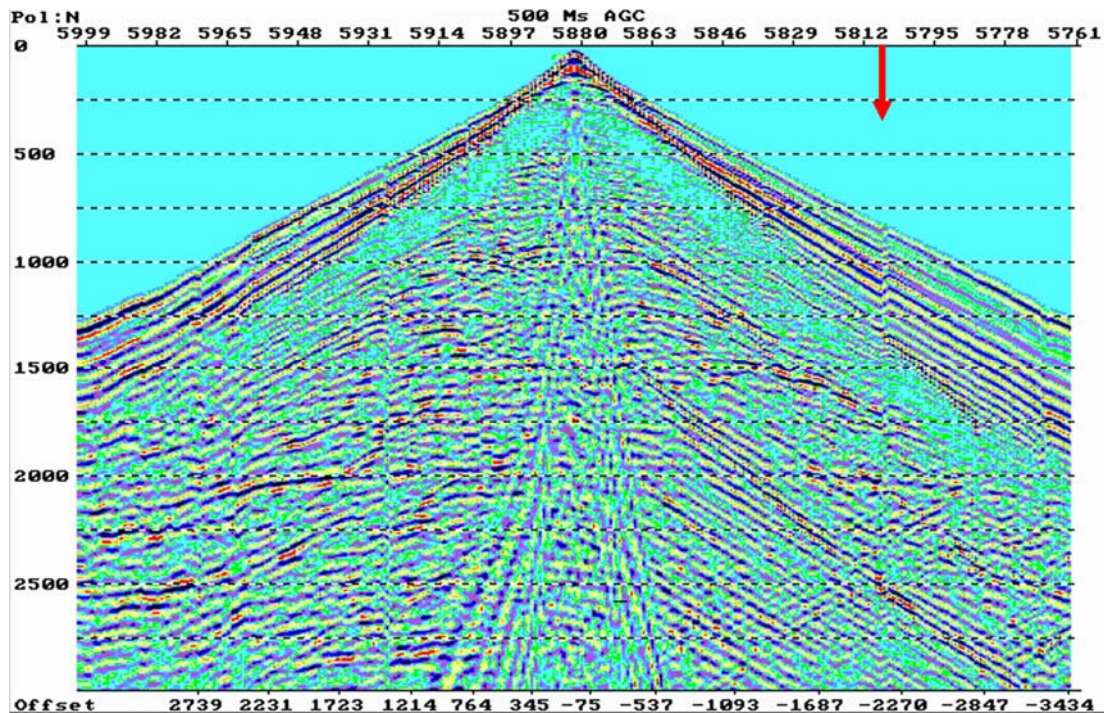


Figure 26. Another shot from the same 2D line as figure 25, but 720 meters further up the line towards the scattering points.

The shot record in figure 26 comes from the same line as the one in figure 25 but from 720 meters further up the line (about equivalent to trace 192 indicated by the red arrow in figure 25). The shot in figure 25 comes from a point about equivalent to trace 5808 indicated by the red arrow in figure 26). Although the two shots are only 720 meters apart, the reflections are quite clear in figure 25 but masked by scattered noise in figure 26.

In figure 26 the shot has moved into an area where there are many scattering points surrounding the seismic line. The many intersecting hyperbolae become less distinct and the initial impression is that this record has a high level of “random” noise. However, the noise is repeatable with the shot point. When there is a great deal of scattered source energy throughout a record, we refer to this as chaotically-scattered source-generated noise.

Noise that is random in time is usually considered to consist of all frequencies. Noise that is random in space, we refer to as chaotic and we may assume that it consists of all wavelengths. We say it is broadband in wavelength. It overlaps some longer wavelengths that are consistent with reflection signals and extends into much shorter wavelengths.

Figure 27 shows a model of signal in red that is similar to the model we showed in figure 3. The signal is band-limited to wavelengths longer than 80 meters and can be adequately sampled by a point-receiver interval of 40 meters. But we have also generated some chaotic noise that is somewhat broadband in wavelength. The brown curve in figure 27 shows the sum of signal plus noise. In this model, the total energy of noise (the integral between the curves) is 12 dB lower than the total energy of the signal (the integral under the red curve).

Notice that there is some noise that extends beyond the sampling Nyquist of 80 meters (for a 40 meter point receiver interval) indicated by the vertical black line. This shorter wavelength noise will not be properly sampled and will alias. That does NOT mean that it will not be measured. In fact, it will be measured as if it were longer wavelengths and the aliased amplitudes will contaminate the true long wavelengths in the range longer than 80 meter (to the left of the vertical black line).

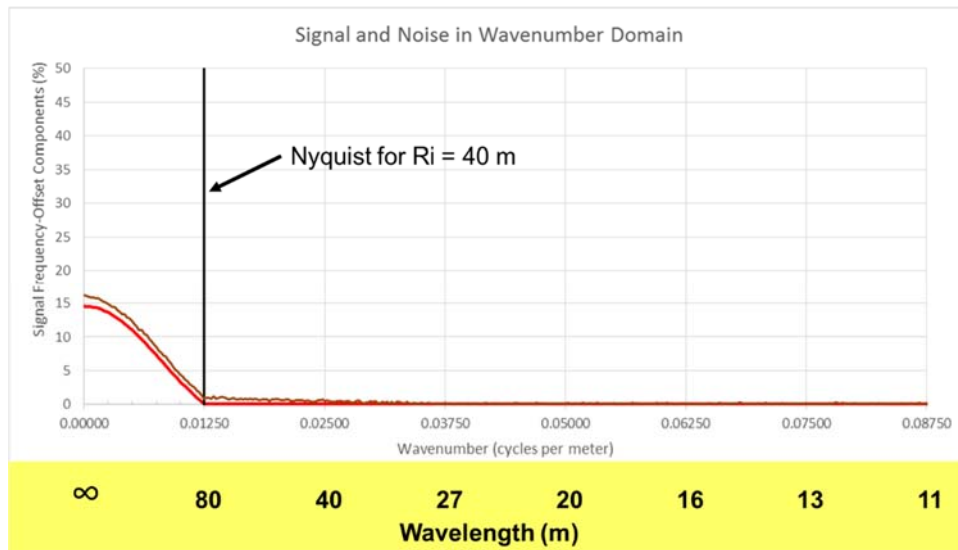


Figure 27. This is a model of the wavelength distribution of signal in red (similar to figure 3), and a small amount of noise that is broadband in wavelength (brown).

In figure 28, we show how all the noise amplitudes with wavelengths shorter than 80 meters will alias and add to the true wavelengths longer than 80 meters. The purple curve is the sum of true signal plus true noise with wavelengths longer than 80 meters plus all of the aliased noise from shorter wavelengths (0.0250 to 0.1250 plus 0.0250 to 0.0375 plus 0.5000 to 0.0375 plus 0.5000 to 0.0625 plus 0.0750 to 0.0625 plus 0.0750 to 0.0875 – all these segments depicted by the orange bar).

Note that the aliased noise decreases the signal to noise ratio in the wavelengths longer than 80 meters. But in this case the signal to noise ratio is still very strong.

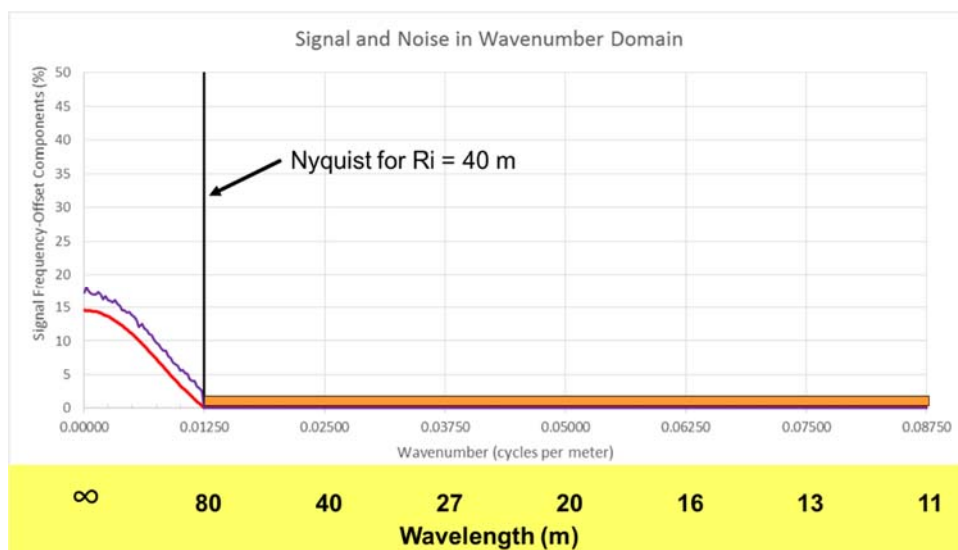


Figure 28. But if the data in figure 27 is recorded using a 40 meter receiver interval, then all the noise at wavelengths shorter than the Nyquist will alias and slightly contaminate the desired signal.

Sub-Sampling of Noise

Now let's consider a model with significantly stronger contributions from noise that is broadband in wavelength. Figure 29 is similar to figure 27, except in this case the total energy of noise (the integral below the blue curve) is 12 dB stronger than the total energy of the signal (the integral under the red curve). In this display, we are showing the noise and signal independently. We have not added the signal level to the noise level.

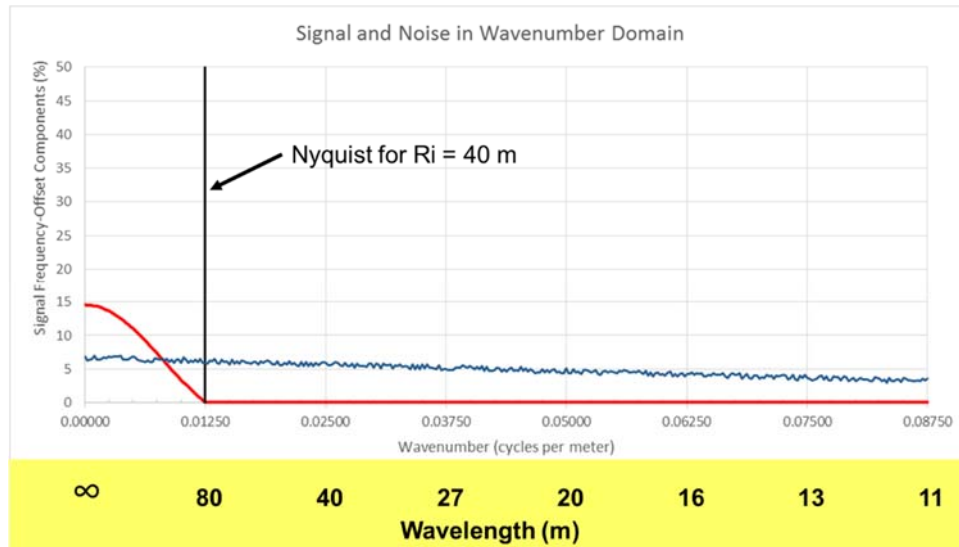


Figure 29. This is a model of the wavelength distribution of signal in red (similar to figure 3), and a fairly large amount of noise that is broadband in wavelength (blue).

Once again, figure 29 shows the noise extending past the sampling Nyquist for 40 meter point receiver intervals. But this time, the noise that will alias is substantially stronger. Figure 30 shows the amplitude spectra of the signal only (in red) and the signal plus noise including all aliased noise (in purple). Note that the noise dominates the signal at all wavelengths of interest.

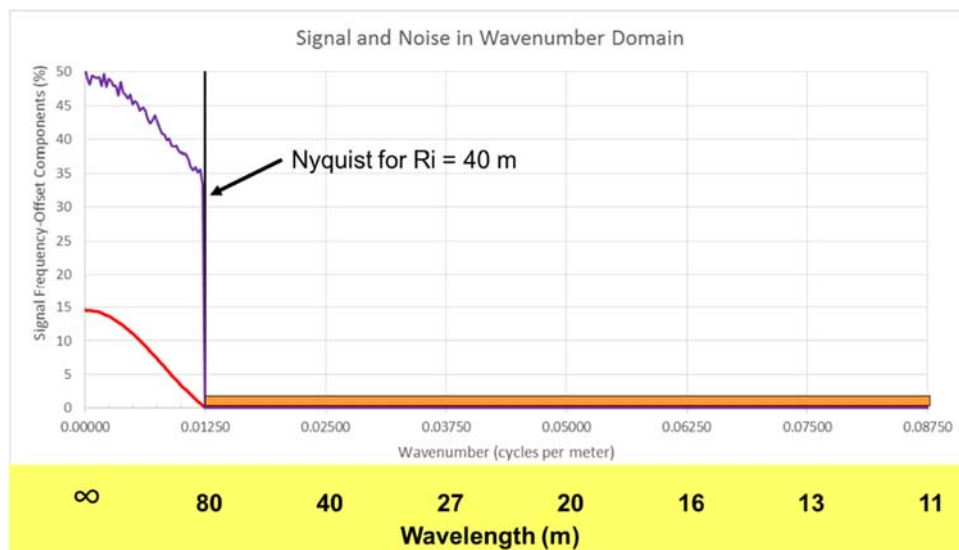


Figure 30. If the broadband noise is strong, then the sum of all aliased components creates a very strong contamination of the desired signal wavelengths.

When chaotically-scattered source-generated noise is strong, then we must make every effort to minimize the effects of aliased wavelengths of noise shorter than the sampling Nyquist. Although a 40 meter point receiver interval is adequate for sampling signal wavelengths, it is too large for sampling the noise wavelengths.

One solution is to reduce the receiver interval. Since the shorter receiver interval is smaller than necessary for sampling desired reflection signals, we refer to this as “Sub-Sampling”. Note in figure 31 that a shorter receiver interval causes the Nyquist wavelength to move to shorter wavelengths. This means there will be less area of noise to the right of the Nyquist that will alias and also the aliased wavelengths will be distributed over a broader range of wavelengths to the left of the Nyquist. The result is that the noise is reduced in the important wavelengths (longer than 80 meters) compared to figure 30.

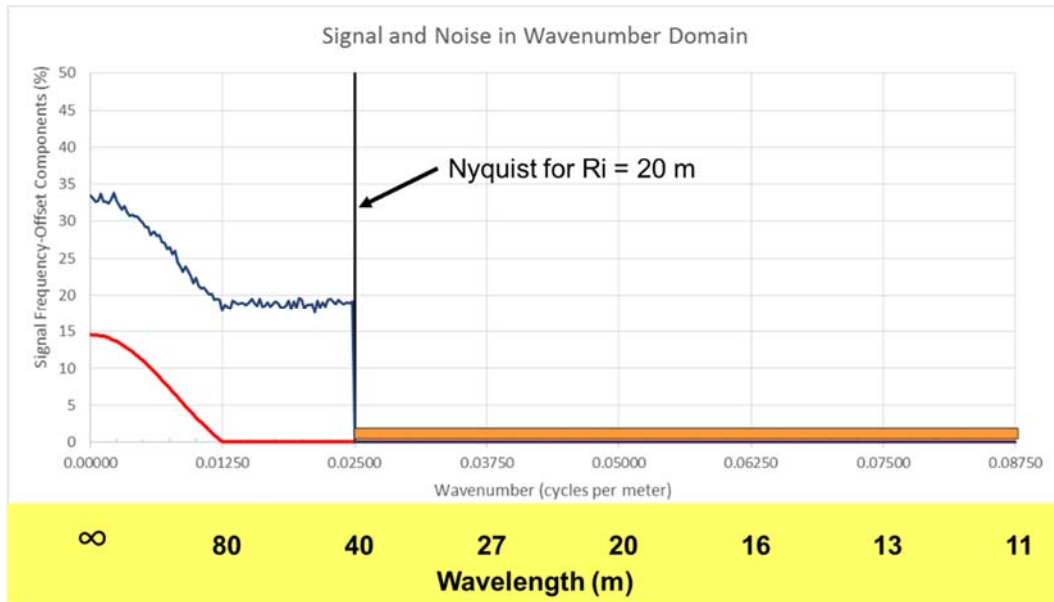


Figure 31. The vertical black line indicates the Nyquist wavenumber for a point receiver interval of 20 m.

In figure 32 we show the effect of reducing the receiver interval to one third of the original shown in figure 30. This further reduces the noise within wavelengths longer than 80 meters, where we hope to recover the reflection signals.

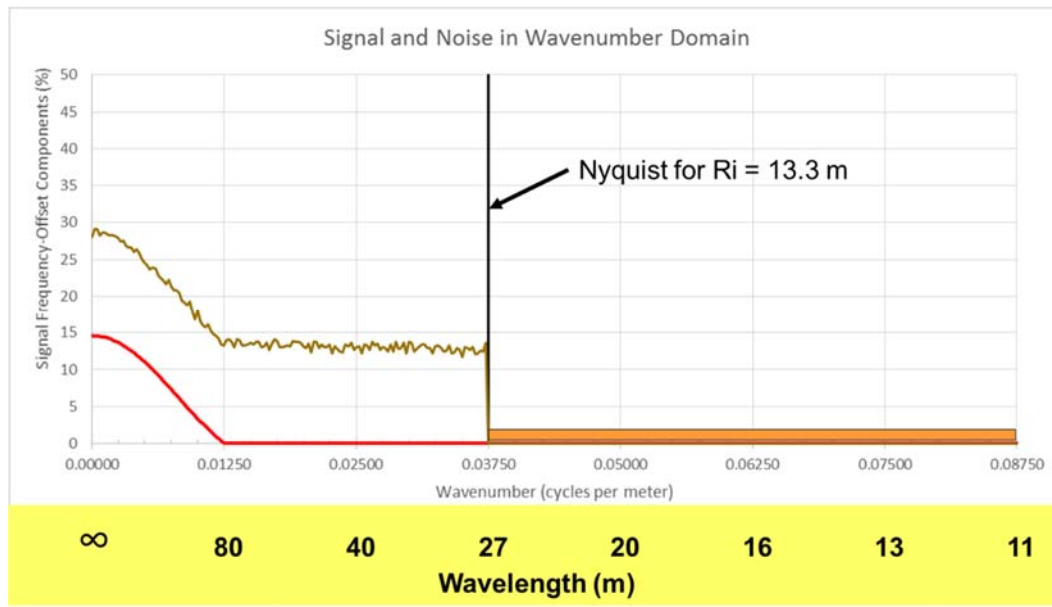


Figure 32. The vertical black line indicates the Nyquist wavenumber for a point receiver interval of 13 m.

In areas where short wavelength noise is significant (usually due to chaotically-scattered source-generated modes), then some form of spatial sub-sampling is absolutely necessary.

Many geophysicists mistakenly believe that the move towards single point receivers means replacing an array of geophones that produces one recorded trace with a single point receiver every 40 meters. This may be acceptable if we are certain there will be no short-wavelength noise throughout the prospect. However, in the presence of short-wavelength noise, the receiver interval should be shortened to one half or one third of the originally planned receiver interval if point receivers are to be used.

Sub-Sampling in the Source Domain using Arrays

So, how do arrays allow us to use larger receiver intervals without being vulnerable to aliased short-wavelength noise? In figure 33 we consider the effect of distributing six receivers uniformly over 40 meters (a receiver separation of 6.67 meters). This would move the Nyquist wavelength to 13.3 meters as indicated by the vertical dashed line. The red line represents the desired reflection signal. The dark blue line represents the broadband noise that is 12 dB stronger than the desired signal when integrated across all displayed wavelengths.

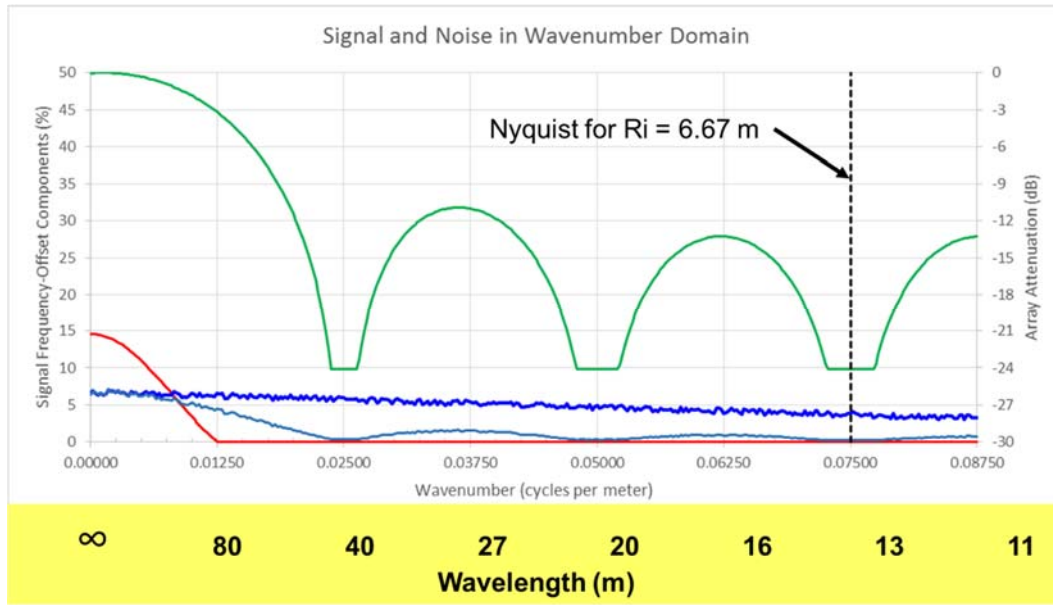


Figure 33. Spatial Sub-Sampling using a 6-element geophone array.

Now, if we sum every set of six geophones to produce one recorded digital trace every 40 meters, summing the spatially distributed elements will produce a wavelength filter that is indicated by the green curve in figure 33 (using the secondary scale on the right side of the plot). The filtered noise is represented by the light blue curve.

After summing, the new spatial sample interval is 40 meters and the light blue noise levels in figure 33 will alias into the wavelengths to the left of the black line in figure 34. The red curve in figure 34 is still our desired signal and the light blue curve is the combined signal, noise and aliased noise after the application of the array. Compare figure 34 to figures 30, 31 and 32. It is clear that the array provides a combination of sub-sampling and filtering that results in a better signal to noise ratio compared with one-half or one-third sub-sampling with point receivers.

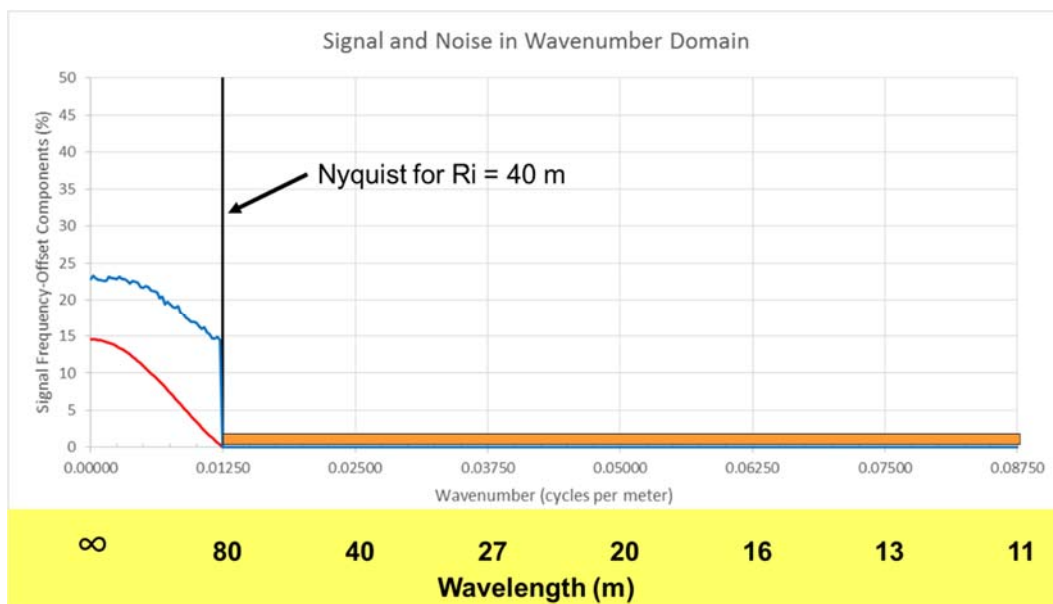


Figure 34. Signal plus noise plus aliased noise using a 6-element geophone array.

All of the previous examples were based on the assumption that all signal wavelengths were 80 meters and longer and that a 40 meter receiver interval would be sufficient to capture all signal of interest. Of course, we generally use shorter intervals in 2D acquisition, but all of the above displays would be the same for 20 meters signals with shorter arrays and only the wavenumber scale would change.

The following displays show a comparison of various point receiver and array configurations for real 2D data. This data was recorded in northeast Alberta using single sensors at one meter intervals. Figure 35 shows the full data set for three source points. Note that there is moderate coherent source-generated noise as well as some chaotically-scattered source-generated noise. The diagram of geophone disposition at the bottom of the display does not match the horizontal scale of the trace display in the top part of the display. It is a much more detailed depiction of the geophone locations over a few stations.

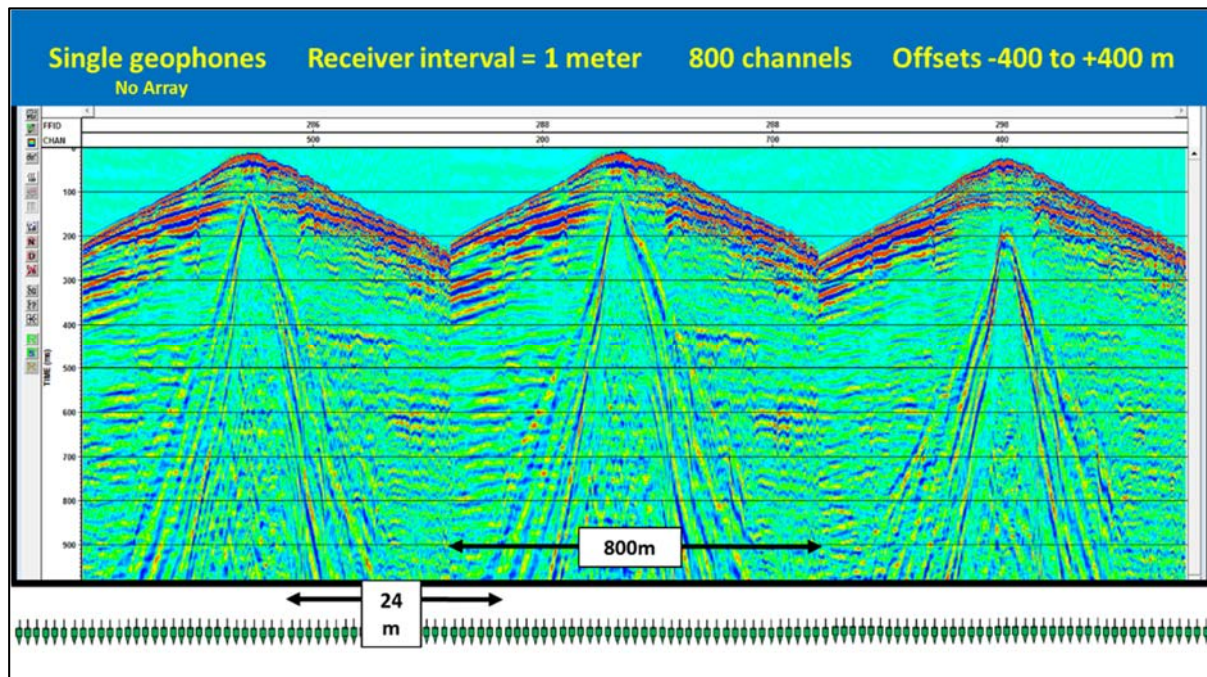


Figure 35. Three shot records using point receivers with 1-meter receiver interval.

Figure 36 shows the same data using every 24th trace. This is the data that would be recorded using a point receiver with a 24-meter receiver interval. Compare this with figure 37 that shows the result of the averaging of 6 traces at 4-meter spacing to produce one trace every 24 meters. This simulates the output of a 6-element array uniformly distributed over the 24 meter receiver interval.

Notice that the strong coherent linear noise is still evident. The purpose of the array is NOT to filter those noise modes. However, the aliased noise that is quite strong in figure 36 is subdued in figure 37 and reflections become considerably more clear.

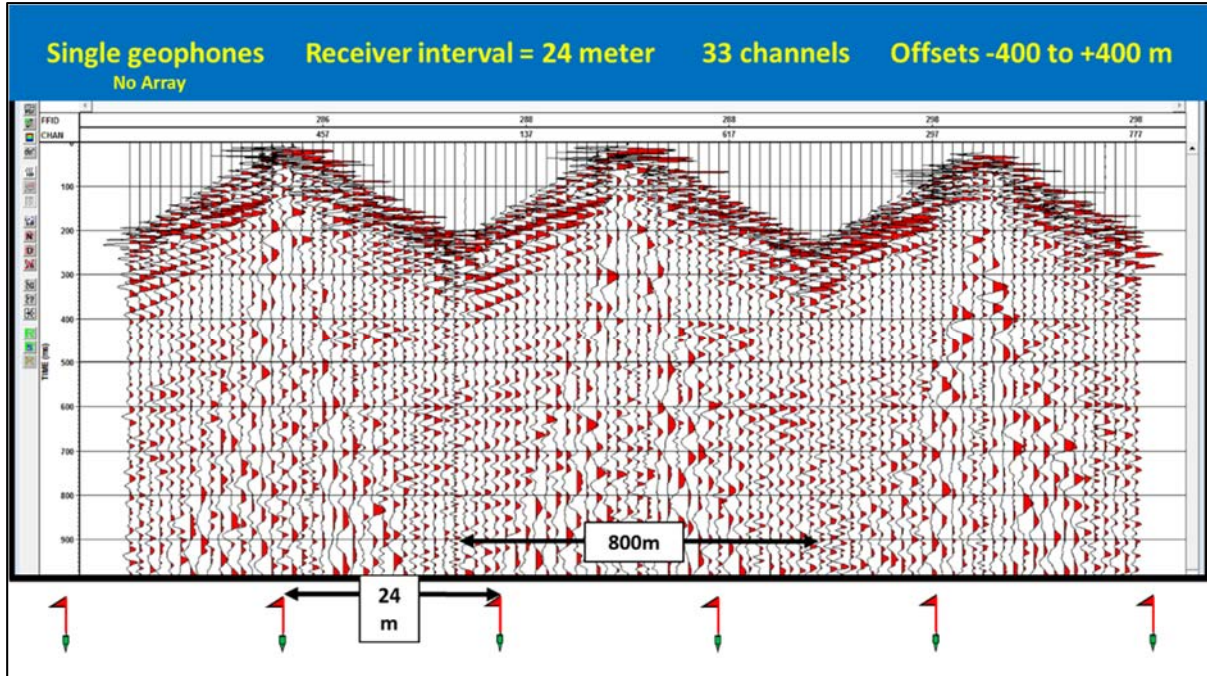


Figure 36. A decimation of the data in figure 35 using one trace every 24 meters.

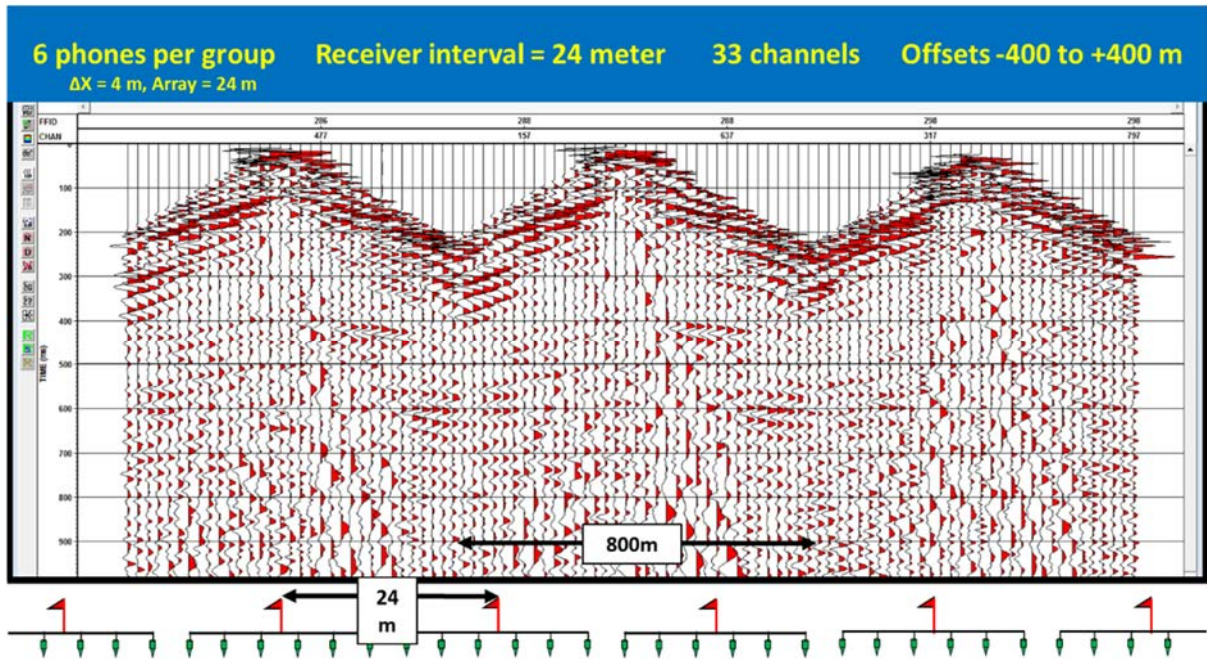


Figure 37. One trace every 24 meters formed from the average of 6 traces with a 4-meter separation.

Figure 38 simulates a “Podded” array where six geophones are closely spaced to produce a recorded trace every 24 meters. Notice that there are no significant differences between the data in figure 38 versus the data in figure 36. “Podded” groups of geophones provide no sub-sampling benefit, no anti-aliasing benefit, and lack the production time advantage of single sensors.

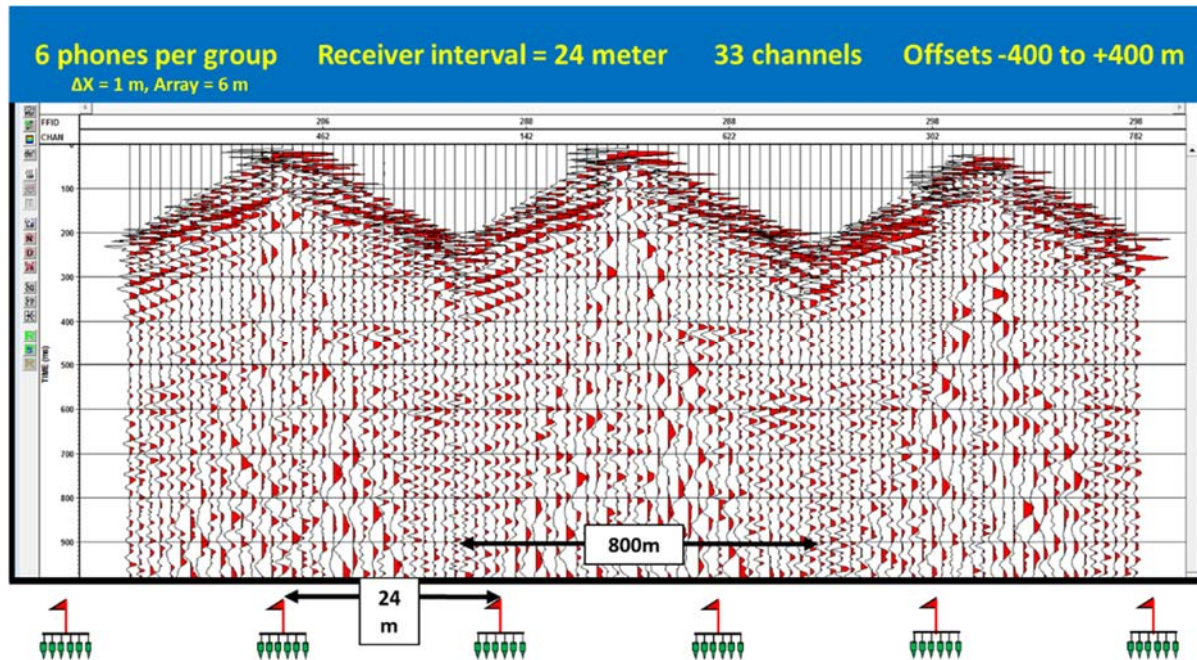


Figure 38. Six-element array with the elements closely grouped over six meters.

The strategy of using “podded” geophones is the worst possible solution to any acquisition problem. Single sensors at sparse intervals are OK only if there is no short wavelength noise that may alias, but they do provide a significant production advantage. Single sensors at much smaller receiver intervals provide sub-sampling advantages that may alleviate the problem of aliased short-wavelength noise. However, the asset cost and production time are increased. Short geophone arrays distributed over the receiver interval can provide interim sub-sampling and suppression of aliased short-wavelength noise. Arrays are often a more economical solution compared with reducing receiver intervals by a factor of three using single sensors and/or nodes.

Figures 39 and 40 show another interesting test of single sensors versus arrays and the impact on final stacked images. The data in figure 39 was recorded in the MacKenzie Delta of northern Canada in the year 2000. Due to the nature of this test the source interval was 20 meters using a vibroseis source, while the receiver interval used was 40 meters.

In other experiments elsewhere in Canada, single sensors buried below muskeg often produce better data than single sensors or arrays of geophones on the surface of the muskeg. In areas such as the Peace River heavy oil deposits where the muskeg is very thick and the buried sensors do not reach below the muskeg, the surface array data provides better stacked results than buried single sensors. In this example (figures 39 and 40), the experiment was conducted in thick recent deltaic sediments. The data from surface arrays is markedly better than the data from the downhole single sensors. In this case, we believe that the downhole sensors were not sufficiently deep to encounter more competent surrounding materials compared to the surface sensors. In this case, the arrays were very valuable in suppressing much of the near-surface chaotic noise.

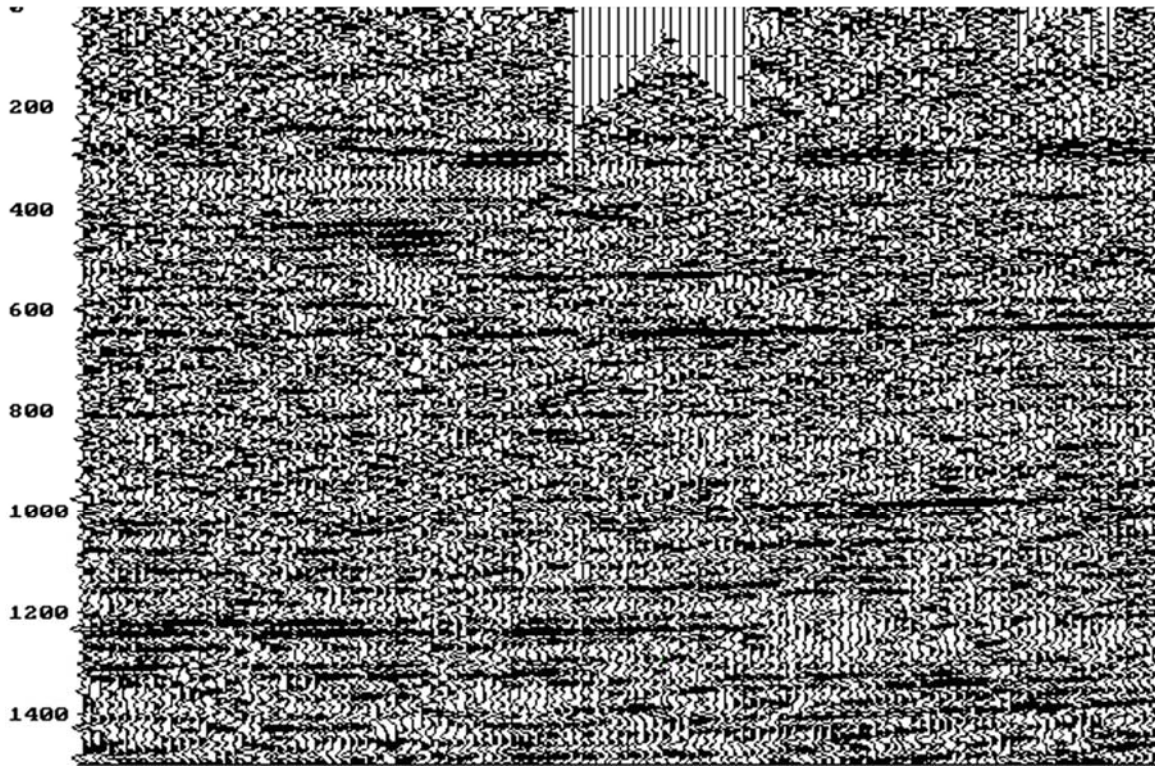


Figure 39. Data recorded using single sensors buried at 20 meters.

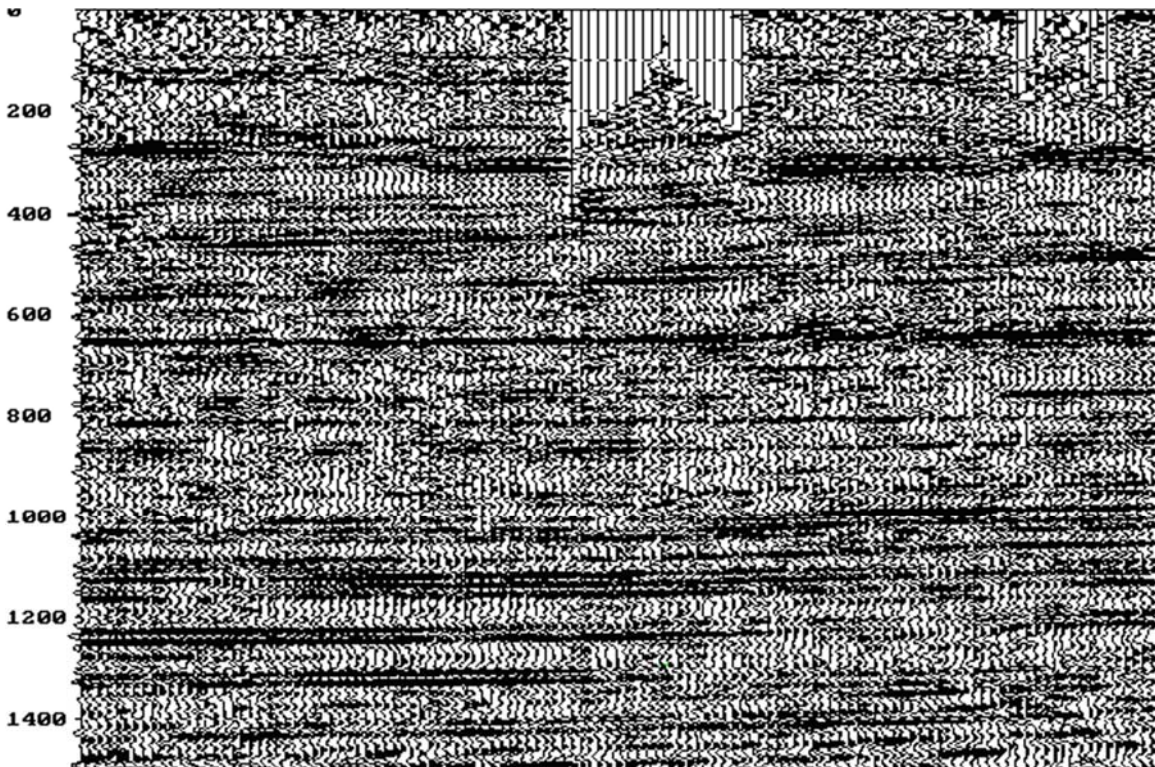


Figure 40. Data recorded using surface arrays.

Arrays and Sub-Sampling in the 2D CDP domain

We must also consider spatial sampling in the CDP domain. Each collection of traces that share common mid-points within a CDP interval is called a CDP gather. We use a “Stacking Chart” to help visualize which traces will have common mid-points. Figure 41 demonstrates how we form a stacking chart. Basically, a stacking chart is an X-Y plot where each recorded trace is represented by a small dot and the dot is plotted according to its mid-point location along the X-axis and its source-receiver offset along the Y-axis. In figure 41, we consider one shot location along a 2-D line (the red circle). We graph three receiver locations (the blue circles) for which we recorded trace data when the red shot location was activated. Each trace will have a different midpoint (indicated by the vertical black lines) and a unique offset. Here we used signed offset (receivers to the right of a shot are called negative offsets, while receivers to the left of a shot are called positive offsets). The small dots at the center of each green circle represent the three recorded traces in the CDP-Offset domain.

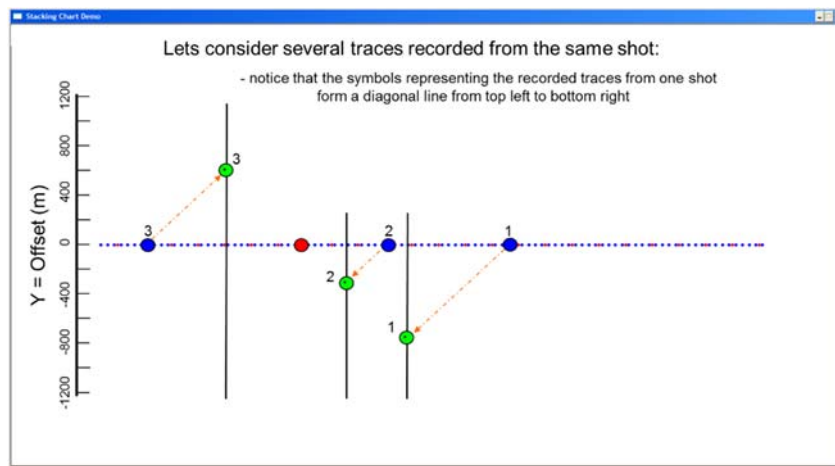


Figure 41. Example of construction of a 2D stacking chart.

Figure 42 shows a more completely populated stacking chart. Notice that all traces generated from a single source point form a collection of points that align diagonally from upper left to lower right. This is called the “common source” orientation. All traces collected along such an alignment form a common source record. You may also recognize that all traces recorded by a single receiver location form a collection of points that align diagonally from upper right to lower left. All traces collected along this alignment form a common receiver gather. Traces collected along horizontal alignments form common offset gather. And traces collected along vertical alignments form common mid-point gathers (what we sometimes also call a CDP gather). Several CDP gathers are indicated in figure 42 by vertical blue lines. There is one CDP gather every half receiver interval.

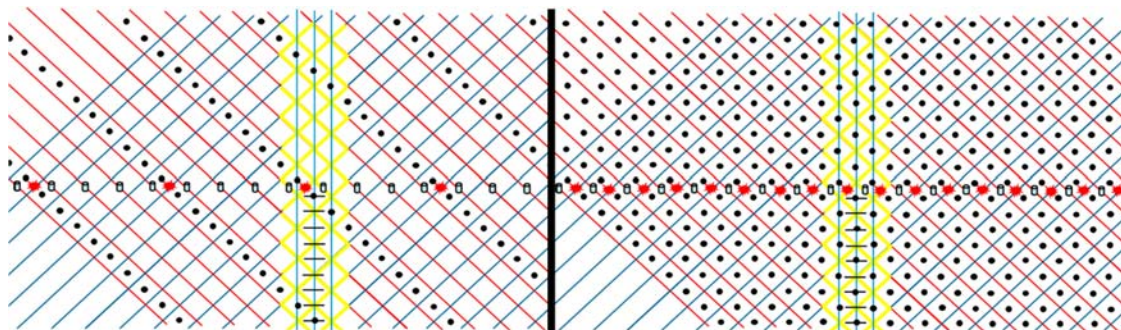


Figure 42. Stacking charts with sparse source interval (left) and fine source interval (right).

The left side of figure 42 shows the stacking chart obtained for a 2D line where the source interval was four times the receiver interval (perhaps 20-meter receiver interval and 80-meter source interval). Notice that in each CDP gather we see a fairly sparse population of black dots. In a regular 2D line, each CDP gather will consist of adjacent traces that are different in signed offset by a distance equal to two times the source interval. Again, a sparse sampling of offsets in each CDP may be sufficient to provide good images of noise-free data. However, if noise is a factor, then we may wish to have finer offset sampling in each CDP. This is obtained in part by reducing the source interval.

The right side of figure 42 shows the stacking chart obtained for a 2D line where the source interval was equal to the receiver interval (generally referred to as “Stack Array” configuration). Notice that the population of black dots in the CDP-Offset domain is much more complete and that each CDP gather contains a better distribution of trace offsets. Every CDP is sampled in offset increments equal to two times the source interval, which is equal to two times the receiver interval.

If the source points are located on the half-station (between receiver points), then the positive offsets will complement the negative offsets and the CDP would be completely populated in un-signed offsets with a trace representing every offset in increments of the receiver interval. If the source points are coincident with receiver points, then in un-signed offset a CDP would contain two samples of every second offset rather than one sample of every offset. This is why it is best to have source points on the half station between receivers.

Figure 43 shows a real stacked data example from east-central Alberta. Both sections were recorded the same day by the same crew using the same equipment. Both sections used a receiver interval of 20 meters. The data on the left was recorded using a source interval of 80 meters and the data on the right used a source interval of 20 meters. This would result in a theoretical fold that is four times greater on the right with an expected signal to noise improvement proportional to the square root of four. However the data on the right is much more than two times better than the data on the left! This is due to the improved offset sampling of the moderate level of chaotically-scattered source-generated noise that is evident in the data on the left.

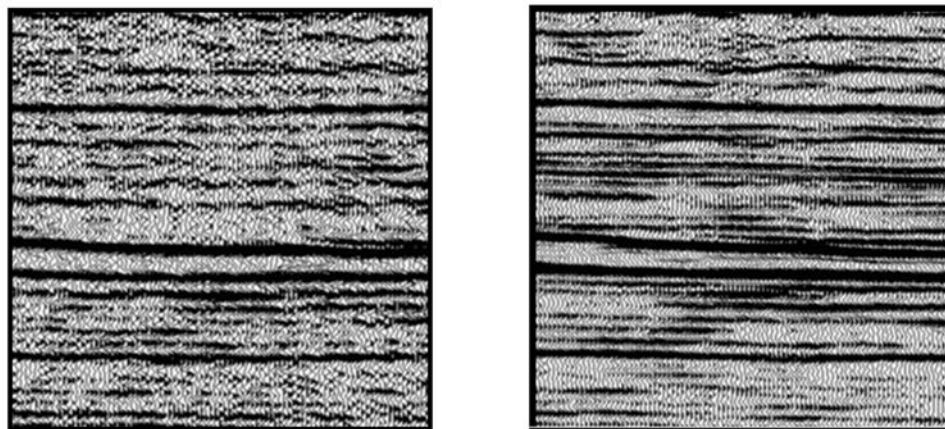


Figure 43. Receiver interval is 20 meters. Source interval is 80 meters on left and 20 meters on right.

In fact, the source parameters for the data on the left used 4 vibrators doing a 4 sweeps every 80 meters. The data on the right used 1 vibrator doing 2 sweeps every 20 meters. The data on the right would be better by a factor of two according to theory relating to fold. However, the data on the left should be better by a factor of four according to theory relating to number of vibrators used. And the data on the left should be better by a factor of 1.4 according to theory relating to the number of sweeps summed per source point. But all of that theory assumes the noise is time-variant, random and Gaussian-distributed in amplitudes. For noise that is chaotic and source-generated, it is most important to have fine offset sampling of traces within each CDP gather.

But the stacking charts we have examined so far show only one black dot for each source-receiver trace. This assumes that we are using point-sources and point-receivers. This is represented by the detailed diagram on the left of figure 44. Each yellow diamond represents one CDP-Offset “Bin”. This is the area within which traces will be collected to form one recorded trace.

If we consider a 6-element geophone array that is uniformly distributed over one receiver interval, then each receiver of the array will produce a unique mid-point and offset. This is represented by the middle diagram of figure 44 where each recorded trace will now be formed by averaging six traces that provide six diverse measurements of short-wavelength noise. If we also consider a 3-element source array we will get 18 individual elements combining to create each recorded trace. Whatever the calculated CDP fold for this 2D line, the application of source and receiver arrays will increase the effective trace density by a factor of 18. While this may not be necessary or beneficial in noise-free areas, it can be VERY beneficial in areas plagued by short-wavelength noise modes.

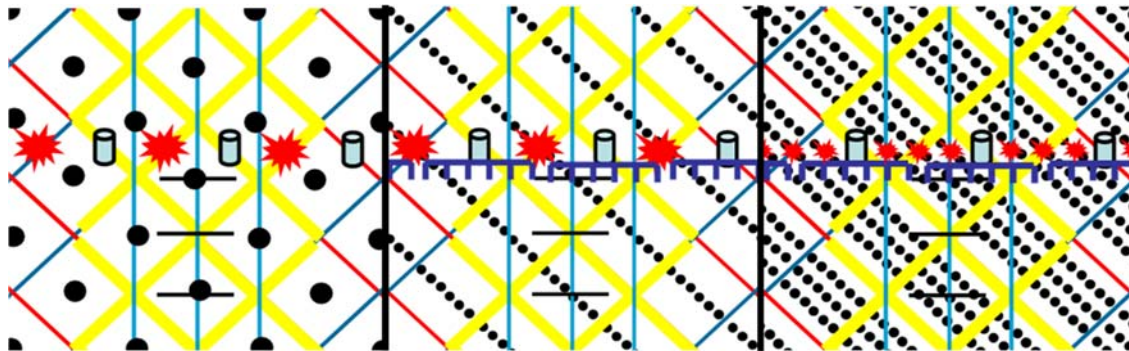


Figure 44. Mid-Point and Offset distributions for point-receiver and point-source (left); 6-element receiver array with point-source (middle) and 6-element receiver array with 3-element source array (right).

Figure 45 shows a detail of just one of the CDP-Offset “bins” shown on the right side of figure 44. Note that each diamond-shaped bin is 20 meters across (in mid-points) and 20 meters vertically (in offset). Point-source and point-receiver recording would produce one measure per bin (20-meter spatial sample interval in offsets). The combined arrays produce 10 weighted measures in the same bin (2-meter spatial sample interval in offsets).

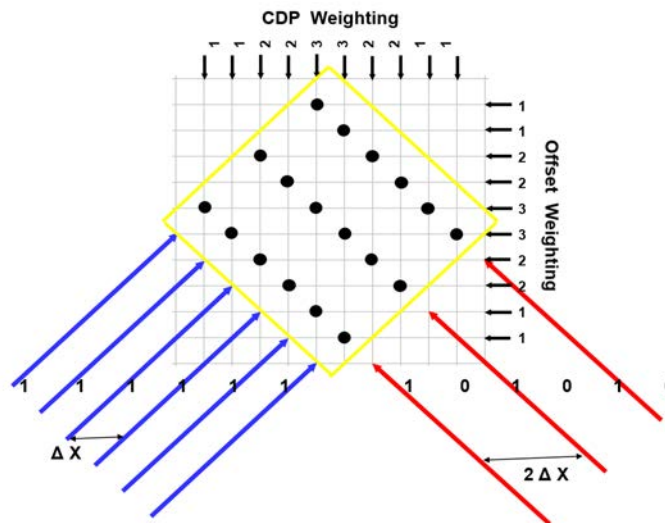


Figure 45. Detail of element distribution for receiver and source array within one CDP-Offset bin.

The individual element samples also result in a distribution of points across the mid-point axis. These points will be summed in the field without NMO or statics corrections. However, if mixing data across such a short distance is a concern, then obviously the selected receiver interval is too sparse to properly measure the expected geologic rate of change spatially.

In figure 33, we showed the array response (green curve) for an array uniformly distributed over one receiver interval. At the receiver interval sampling Nyquist (80-meter wavelength in figure 33) the attenuation due to the array (the normal move-out assuming straight-ray theory) is three decibels. This is at the Nyquist limit of spatial sampling for the given receiver interval. We should be designing our receiver interval to safely protect all signals of interest well to the left (longer wavelengths) of the Nyquist limit. Therefore, an array distributed over one receiver interval should never yield a significant attenuation (due to normal move-out) of signals for which the receiver interval was designed.

Since early work by Nigel Anstey and others, it has been well understood that four factors will contribute to a technique referred to as “Stack Array” and will provide optimum data quality in 2D seismic. In rank of importance the four factors are:

1. The source interval should be equal to the receiver interval
2. The source should be centered on the half station (between receiver centers)
3. A receiver array uniformly distributed over one receiver interval
4. A source array uniformly distributed over one source interval

Many authors have claimed that the purpose of arrays in past applications has been to attenuate ground roll and other slow-moving low-frequency linear noise modes. For myself and other adherents to the stack-array concept, **this has never been true.**

Most ground roll and shear waves have a range of wavelengths that extend into the range of some of the wavelengths of reflection signals. To filter ground roll in the field inherently means also filtering desired signal. The first tenet of filtering should be to design filters to pass signal, NOT to attenuate noise. Therefore, an array equal to or shorter than the designed receiver interval should pass all desired signal provided the receiver interval was correctly selected.

Again, the prime purpose of arrays is to sub-sample the receiver interval that was designed to measure desired signals and to provide anti-alias filtering of shorter wavelengths of noise.

It has also been stated by those who argue against arrays that the use of arrays attenuates desired high-frequency signals. In the past, some programs have used very long arrays, and for such cases this statement is entirely true. However, in our applications of arrays, we recommend only short arrays. For 2D programs we do not recommend an array longer than the chosen receiver interval. For 3D programs, we recommend arrays with effective length equal to one-third of the chosen receiver interval. We combine this with our “triple stagger” design to get continuous sub-surface mid-point sub-sampling (to be demonstrated later in this paper).

Figure 46, shows the responses of two arrays. We know from figure 1 that apparent wavelength is a function of reflector depth, RMS velocity, source-receiver offset and frequency. In the images in figure 46, we have fixed the depth at 1200 meters and the velocity at 3600 m/s. The array attenuation is a function of apparent wavelength, which is a function of offset (along the X-axis) and frequency (along the Y-axis). The vertical black line is set to an offset of 1400 meters (a generous estimate of the maximum available offset for a reflector at 1200 meters). The tick marks along the vertical black line reproduce the frequency scale indicated at the left of the plot. The color indicates the amount of signal attenuation due to a 6-element array. The attenuation scale runs from pure red (zero attenuation) to pure blue (4 decibels or more attenuation).

The upper part of figure 46 represents the response for a long array (80 meter effective length). Notice that only the very near offsets do not suffer from high-frequency attenuation. The far offsets experience 4 decibels of attenuation or more above 60 Hz. This is certainly not desirable.

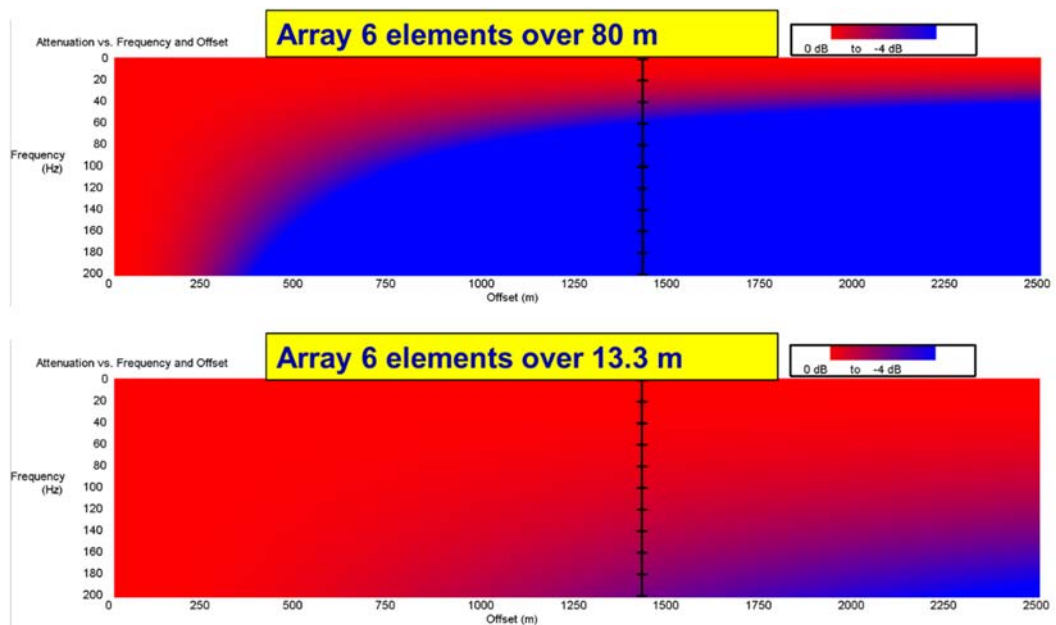


Figure 46. Array attenuation as a function of source-receiver offset and frequency.

However, the lower part of figure 46 shows the same response but for a short array using 6 elements separated by 2.67 meters (effective length of 13.3 meters). This is the length of array we would recommend for a 3D program designed with a 40-meter receiver interval. In this case, all offsets from 0 to 1400 meters and all frequencies from 0 to 200 Hz experience less than 3 decibels of attenuation. This array will not be destructive to desired reflections signals from the target depth, but it may be very helpful in sub-sampling and anti-alias filtering of short-wavelength noise modes.

The array responses depicted in figure 46 (or by the green curve in figure 33) show array attenuation due to the spatial distribution of elements along a flat surface. These responses take into account the differential move-out for ray paths emerging at the nearest element in the array versus the farthest element in the same array. Another way of expressing this is the average of wavelets that experience a phase difference due to differing travel path distances. Some geophysicists seem to think that NMO and phase changes act in addition to normal array response curves. However, these are exactly the physical phenomena that are calculated and accounted for in the response curves.

The array responses presented so far in this paper assume a flat surface, flat reflector, homogeneous and isotropic material between the surface and the reflector. These assumptions, of course, do not often occur in real situations.

Figure 47 shows a slightly less simple model where velocity increases with depth. This is much more typical of most sedimentary basins. This will result in curved ray paths (as shown in solid brown lines) as opposed to straight ray paths (as indicated by the dashed red lines). Note that as a curved ray emanates or emerges at the surface, the angle of emergence is less than for straight rays. This means that curved rays will exhibit longer apparent wavelengths compared to straight rays. Therefore, if we use straight ray theory to predict the shortest wavelength of signal, we suspect that actual signals will not reach this limit. Any array designed to protect signal wavelengths calculated using a single homogeneous layer, will certainly protect more realistic reflections. In other words, our array response curves underestimate the width of the first pass band and overestimate the attenuation at the receiver interval Nyquist.

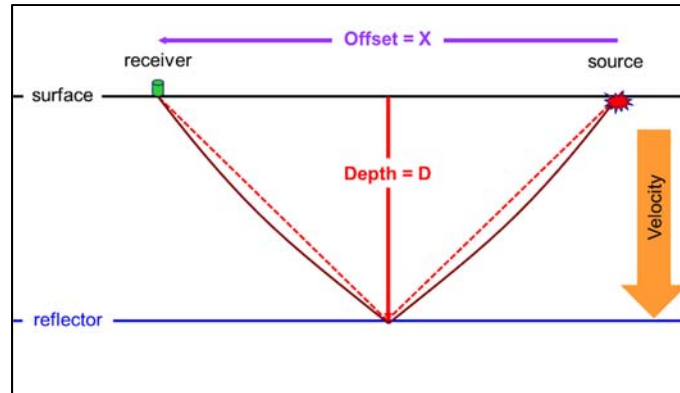


Figure 47. Curved rays occur when velocity increases with depth.

Another concern is what happens at the near surface if topography or near-surface velocity variations result in static shifts for data arriving at one geophone versus others within the same array. These are referred to as “In-Group Statics”. Since the outputs of geophone elements within an array are averaged without the benefit of statics adjustments, this could result in mis-stacking of higher frequency components.

We created 600 traces with a single reflection coefficient. We filtered that spike with a zero-phase Ormsby wavelet of 10-15-200-250 Hz to simulate a broadband reflection. We then introduced random statics ranging from -2 ms to +2 ms. Then successive groups of six traces were averaged to produce 100 traces. Each trace represents the output of a 6-element array where in-group statics vary over a 4 ms range. A composite image showing those 100 simulated array outputs is reproduced in figure 48.

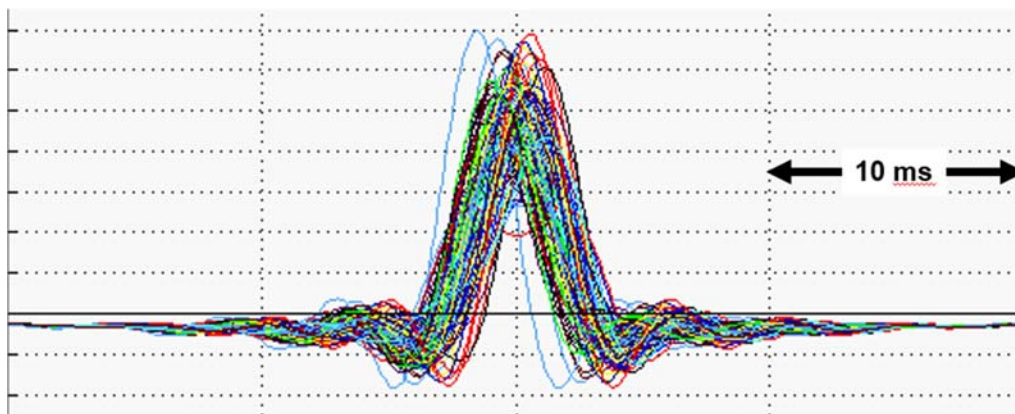


Figure 48. 100 repetitions of a 6-element array averaging a 10-15-200-250 Hz wavelet with +/- 2 ms statics.

In figure 49 we show the effect of 4 ms statics on the 100 wavelets in the frequency domain. Notice that some wavelets are not effected very much while some are more significantly filtered. The heavy dashed black curve shows the average response. At 100 Hz, the maximum effect is 6 decibels of attenuation while the average is only 2 decibels. In a 100 fold CDP stack, we would expect the net effect of in-group statics to be represented by the average curve in figure 49. We would expect 3 dB of attenuation of signal amplitudes at 110 Hz. We see this as relatively minor provided the use of the array for sub-sampling and anti-alias filtering of short wavelength noise has more significant value.

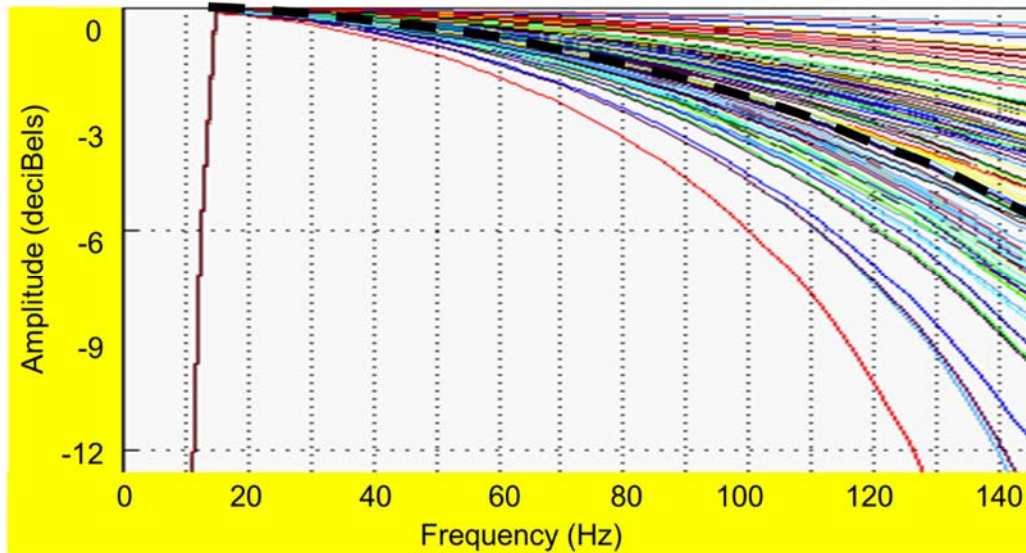


Figure 49. Amplitude spectra for the 100 wavelets in figure 48.

We have conducted many tests in a variety of basins and noise conditions using single sensors at one meter intervals. We very seldom see in-group statics of 4 milliseconds over short intervals (20 meters and less). Using ray theory, we can envision such statics over short distances. But keep in mind that in wave theory, the returning reflected wave front may have wavelengths in the order of 20 to 40 meters. A continuous wave front tends to heal very short wavelength variations in a reflected wave and thus limits the magnitude of expected static over short distances.

There are some conditions where in-group statics may be expected to be greater than in others. For example, Karst surfaces where limestone and dolomite at surface may result in heavy fracturing and sink holes. However, these conditions also lead to very severe chaotically-scattered source-generated noise, so sub-sampling becomes even more critical.

Sub-sampling using single sensors and reducing receiver interval to one half or one third may not be sufficient. Single sensor traces tend to be quite noisy compared to the average of six geophones in an array. Noise alters the phase of the reflected wavelet and in severe cases may cause problems for automatic statics programs. One example from Christina Lake area of northeastern Alberta is presented in the following images.

Figure 50 shows a segment of a 2D line that was recorded with a 6-meter receiver interval using analog arrays of six elements uniformly distributed with 1-meter element spacing. The source interval was 12 meters. The green boxes show areas where this section provides better reflection continuity and signal-to-noise ratio compared with the section in figure 51. The section in figure 51 was recorded with a receiver interval of 1 meter using single sensors. The data was processed to CDP intervals of 0.5 meters using similar processing to the section in figure 50. For the display in figure 51, we then averaged 6 adjacent traces after stack in order to produce a 3-meter CDP interval. We also viewed a section using just every sixth trace, but that looked considerably worse in the areas highlighted by green boxes.

It is quite clear that in the highlighted areas, the data produced using arrays yielded a better result than that recorded and processed using single sensors. When we examined the poor data areas, we found the raw traces to be very noisy, particularly on the single-sensor data. When we examined the trace-to-trace automatic statics solutions, we found the single-sensor data produced quite erratic statics in this area. Our conclusion was that the noise single-sensor data resulted in poor quality correlation functions and erratic static solutions during residual and CDP trim statics. So if an area generates very noisy data, single-sensor data may not be able to achieve meaningful statics solutions. Even though an array may result in some loss of frequency content due to in-group statics, it may provide a better over-all solution than noisy single-sensor data.

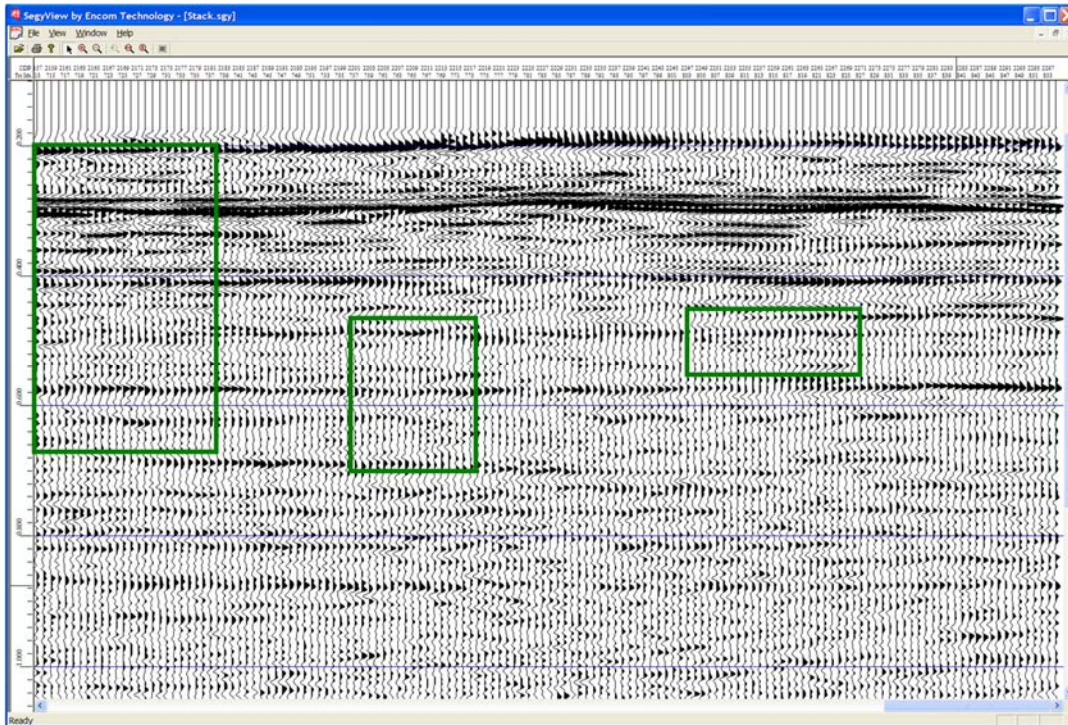


Figure 50. Stacked 2D section using data from 6-meter analog arrays with 3-meter CDP interval.

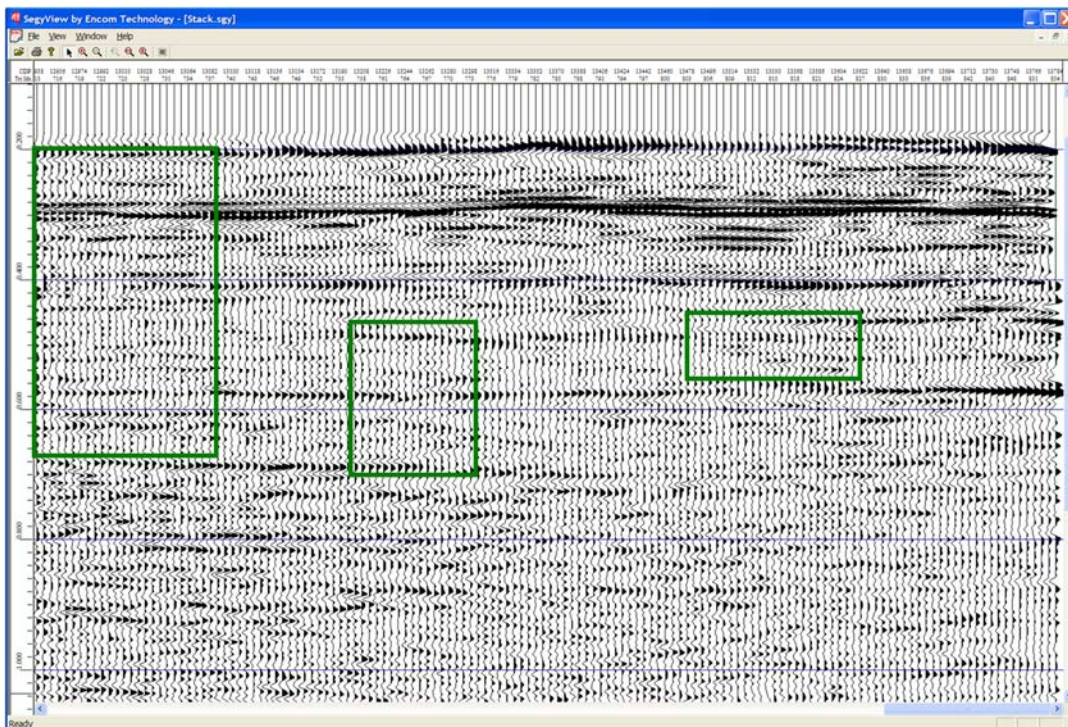


Figure 51. Stacked 2D section using 1-meter trace spacing through all processing, including automatic statics, then averaging groups of six traces to yield 3-meter CDPs.

Arrays and Sub-Sampling in 3D

We also employ spatial sub-sampling in the CDP domain in our 3D designs. In the example below, we have designed a 3D program using:

Receiver interval	= 48 m
Source interval	= 48 m
Receiver line spacing	= 288 m
Source line spacing	= 240 m
Patch	= 22 x 180
Patch Area	= 6636 x 8640 m
Nominal Fold	= 198 in bins of 24x24 m
Fold in offsets 0-2530 m	= 72.7 in bins of 24x24 m

This design should yield 72.7 fold using traces limited to offsets from 0 to 2530 meters and when collected in natural sub-surface bins of 24x24 meters. If a mid-point focused design is used then each bin will contain an average of about 73 mid-points all coincident at the center of each bin. Assuming the survey uses point receivers and point sources, then the trace density would be 126,271 traces per square kilometer using offsets 0-2350m.

Figure 52 shows the midpoint distribution for such a design. The red line is a source line and two point sources are shown 48 meters apart. The blue line is a receiver line and two point receivers are shown 48 meters apart. The light black squares represent the natural sub-surface bins of 24x24 meters. The heavy black grid in one of the bins shows a sub-division of a natural bin into 8x8 meter sub-bins, but only the center of these is populated.

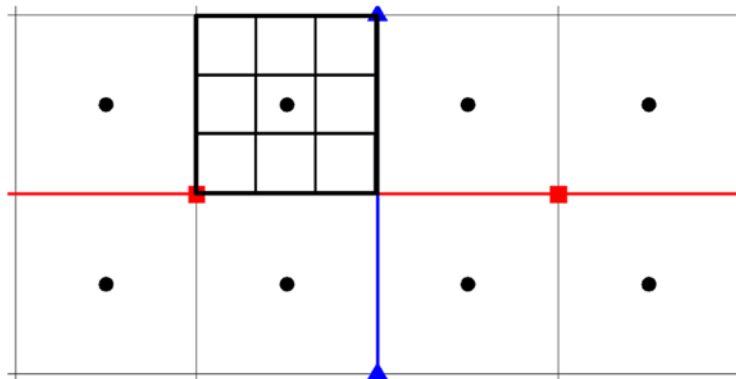


Figure 52. Mid-point scatter for a mid-point focused design using point receivers and sources.

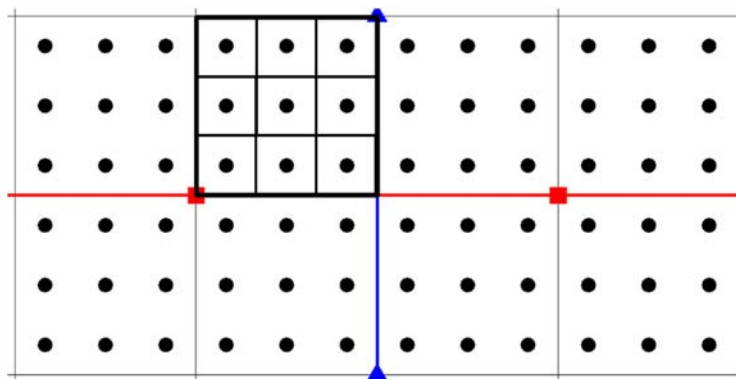


Figure 53. Mid-point scatter for a triple-staggered design using point receivers and sources.

We usually implement a triple-stagger in our designs. The offset of the nearest source or receiver at line intersections is varied from 1/6 to 3/6 to 5/6 of an interval in a repeating pattern. This results in a forced mid-point scatter in natural bins as shown in figure 53.

The natural sub-surface bin is still 24x24 meters and contains mid-points from about 73 pairs of point-source and point-receiver. However, the fold distributed into nine different midpoints within each natural bin. Therefore, we can consider sub-bins of 8x8 meters where each will contain about 8 traces. However, the trace density is still 126,271 traces per square kilometer. The greatest advantage of this method is that we generate more unique mid-point indices and provide better spatial sampling of pre-stack migration operators. With proper recognition of the sub-bin definition, this can result in more generous anti-alias filtering which permits migration of steeper dips and higher frequencies. If we wish, we can generate a pre-stack migrated trace volume in 8x8 meter output bins (or 16x16 m or 24x24 m).

In figure 54, we have replaced the single point receivers with 6-element receiver arrays. In this figure, you can only see the south half of the northernmost array and only the north half of the southernmost array. Each array is centered on the same receiver location as in figure 53. The six elements are uniformly distributed over an effective length of 1/3 of a receiver interval (16 meters) with an element spacing of 2.67 meters.

If we consider the contribution of each individual geophone in the array, we can generate the mid-point scatter plot shown in figure 54. Notice that each point seen in figure 53 is now distributed into six points within each sub-bin in figure 54. We will record the summed output of each geophone array as a single trace, so the recorded trace density is still 126,271 traces per square kilometer. But the actual trace density in the field is 757,628 traces per square kilometer.

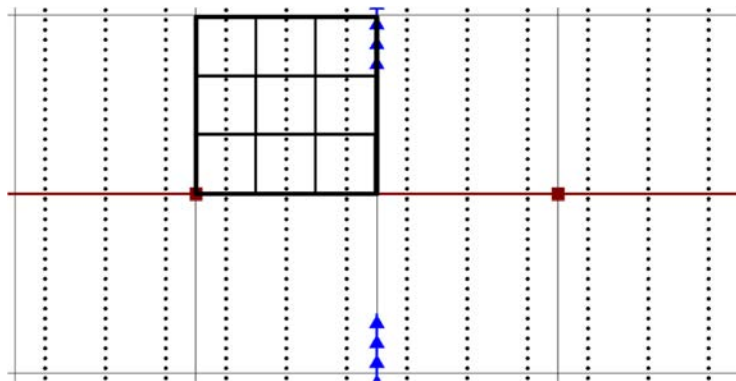


Figure 54. Mid-point scatter for a triple-staggered design using 6-element geophone arrays and point sources.

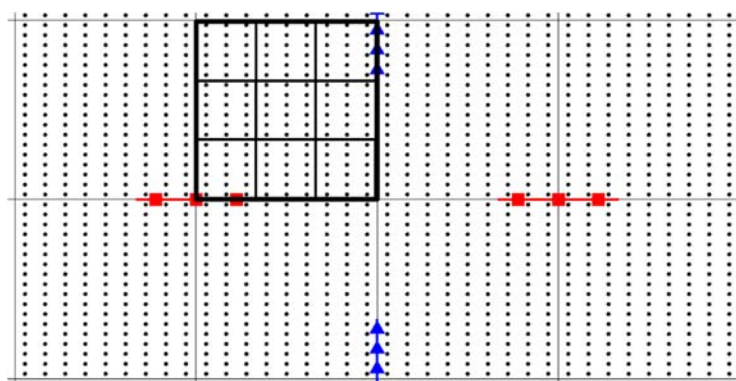


Figure 55. Mid-point scatter for a triple-staggered design using 6-element geophone arrays and 3-element source arrays.

In figure 55, we have replaced the single point sources with 3-element source arrays. Each array is centered on the same source location as in figure 53 or 54. The three elements are uniformly distributed over an effective length of 1/3 of a source interval (16 meters) with an element spacing of 5.33 meters.

If we consider the contribution of each individual source in the array, we can generate the mid-point scatter plot shown in figure 55. Notice that each point seen in figure 54 is now distributed into three points within each sub-bin in figure 55. We will record the simultaneous output of each source array as a single trace, so the recorded trace density is still 126,271 traces per square kilometer. But the actual trace density in the field is now up to 2,272,884 traces per square kilometer.

This is roughly equivalent to producing a survey with the same line spacings but with a point-receiver interval of 8 meters and a point-source interval of 16 meters. That would achieve the same trace density of 2,272,884 traces per square kilometer. However, that would require six times the recording channels, somewhat more acquisition time and much higher processing costs.

Note that potential lateral resolution is usually calculated as a half a wavelength or $V/2F$. For the model we are now considering, the average velocity to the main target may be about 4000 m/s and the highest recoverable frequency may be about 80 Hz (quite optimistic for targets at 2000 meters). The expected limit of lateral resolution then would be about 25 meters. For this reason the design was planned to yield natural subsurface bins of 24 meters. Any attempt to output traces in smaller sub-bins may not improve lateral resolution.

The main difference between the high-density point-receiver and point-source strategy versus the array strategy is that all individual components will be processed independently in the former and sets of 18 components will be averaged in the field in the latter. The array averaging will occur over convolved arrays that represent a surface area of 16x16 meters. Such short arrays will rarely result in any significant frequency loss due to filtering or in-group statics for geologic targets where useable offsets up to 2350 meters are anticipated.

Some geophysicists question the wisdom of using a receiver array in 3D programs where the source may be a point-source. This is very common in dynamite programs and increasingly common in some vibroseis programs.

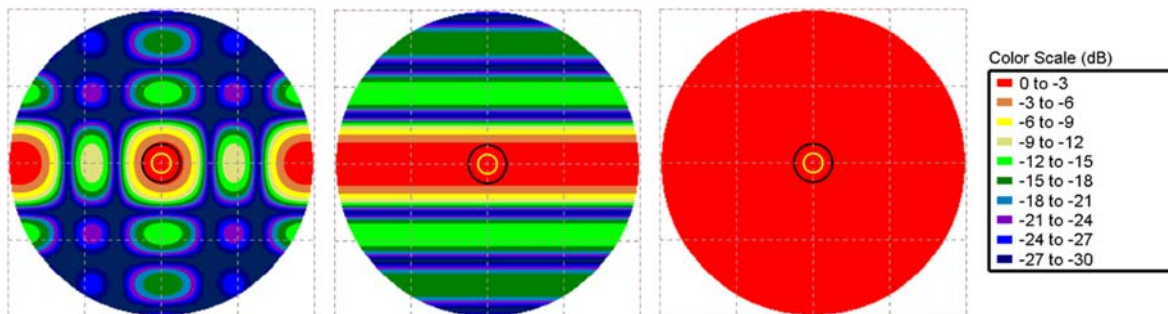


Figure 56. 3D array response plots for receiver and source array (left); receiver array only (middle); and no array (right). Effective length of arrays is 16 meters. The wavelength scale ranges from infinity at the center of each plot down to 5 meters at the outer edge.

In figure 56, we show the 3D array response plots for three situations. These plots show that attenuation due to the array for various wavenumbers (wavelengths) and source-receiver azimuths. The azimuth of any straight line from the center to the outer edge of the plot represents the azimuth from a source to a receiver. The radial distance from the center to the outer edge of the plot represents the wavenumber (inverse wavelength).

Wavenumber ranges along any radius from zero at the center of the plot to 0.2 cycles per meter at the outer edge. In wavelength, this means infinite wavelengths at the center ranging down to 5 meters at the outer edge. The black circle in each plot represents a wavelength of 40 meters and anything outside the black circle is smaller than 40 meters. For the projects we have been discussing, any data with wavelengths outside the black circle are almost certainly noise.

The small yellow circle on each plot represents a wavelength of 80 meters. For most projects, our desired reflection signals lie inside this circle (wavelengths longer than 80 meters). In all three plots, wavelengths longer than 80 meters are protected and experience less than 3 dB of attenuation.

If a receiver array and a source array orthogonal to the receiver array are used, then the plot on left of figure 56 applies. Most of the area representing noise only (outside the black circle) is experiencing some significant attenuation.

If only a north-south receiver array is used with point-sources, then the plot in the middle of figure 56 applies. Much of the area representing noise only (outside the black circle) is experiencing some attenuation. Only traces with source-receiver azimuths from about 80 to 100 degrees or 260 to 280 degrees (more or less east-west) will not experience attenuation.

If no source or receiver arrays are used, then the plot on the right of figure 56 shows that there will be no attenuation of any wavelengths for any azimuth.

Now, remember that for a spatial sample interval of 40 meters, any wavelengths shorter than 80 meters will alias. Those wavelengths will not be measured correctly and they will be misrepresented as longer wavelengths. This means that any noise modes that have wavelengths outside the yellow circle will alias and contaminate the desired signals that lie within the yellow circle. In our recorded data where we have one receiver or one source every 40 meters, we will only recognize signals inside the yellow circle. All information from outside will fold into that small area inside the yellow circle and will distort our ability to recognize the desired reflection signal components.

With no arrays, there is no anti-alias filtering of short wavelength noise. While some geophysicists are fearful of the potential mixing and high-frequency losses due to arrays, they seem willing to make their data vulnerable to a high degree of aliased noise contamination. We have demonstrated that the use of short arrays is not likely to damage the recoverable bandwidth of data, but the averaging suppresses some random noise and provides some protection against aliased short wavelengths of chaotically-scattered source-generated noise.

Increasing Trace Density by Reducing Line Spacing in 3D

In this section, we present a case history from the San Jorge basin of Argentina. Many 3D programs have been recorded in this area with generally good results. However, in certain localized areas, the data deteriorates dramatically and key exploration objectives are not imaged. Figure 57 shows one example of such a situation.

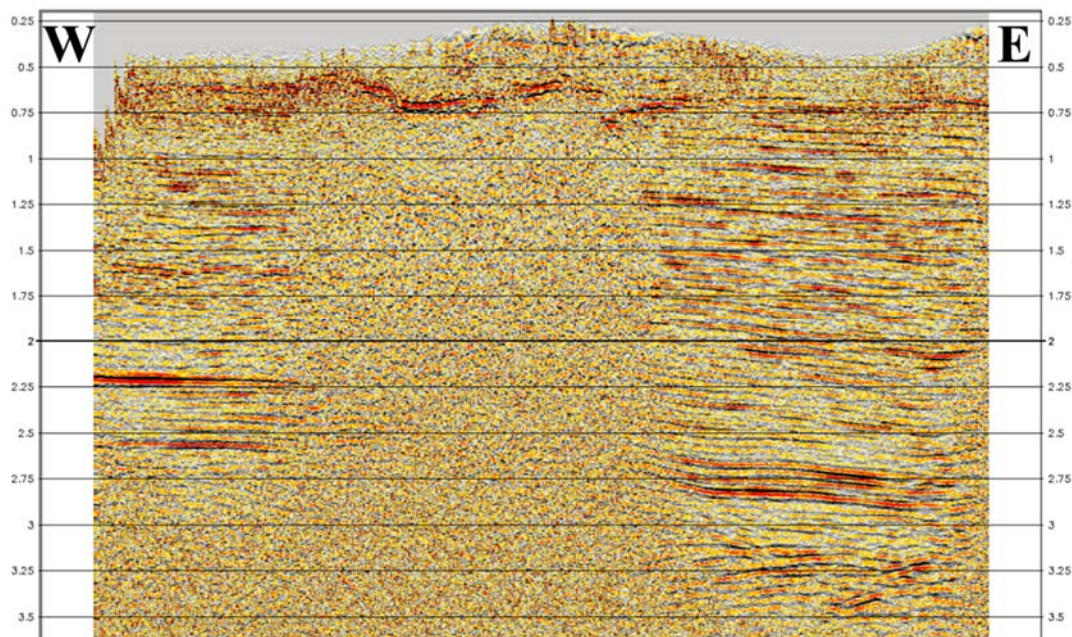


Figure 57. Example of an in-line slice through a 3D volume showing a poor data area amidst good data.

The poor data area in figure 57 lies below some strong and non-continuous reflection segments that are evident between 0.5 and 0.75 seconds. Wells in the area have encountered basaltic intrusive sills at about 500 meters depth in the areas associated with poor data. These sills are somewhat erratic and not correlatable from well to well. It is believed they occur in small overlapping lenses of variable thickness and lateral extents.

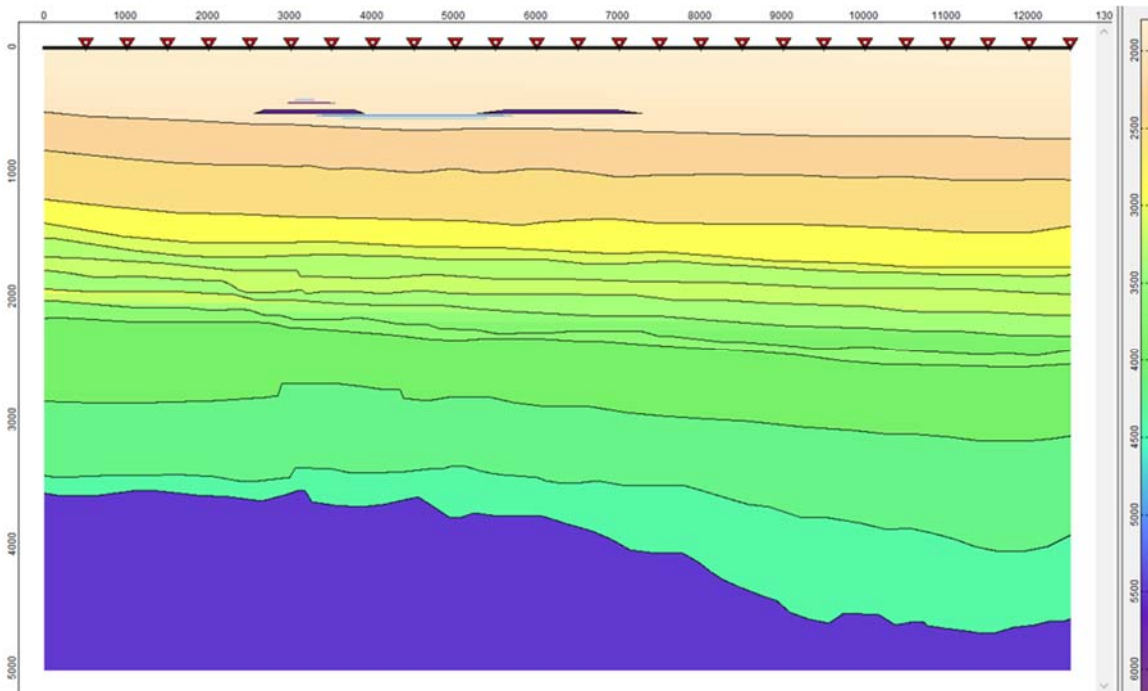


Figure 58. X-T model based on interpretation of the line in figure 57.

Figure 58 shows a geologic depth model of the line in figure 57. At about 500 meters depth we have added some lenses of very fast material representing the basaltic sills. Using Tesseral wave equation modelling software, we generated synthetic shot points from various positions across the surface.

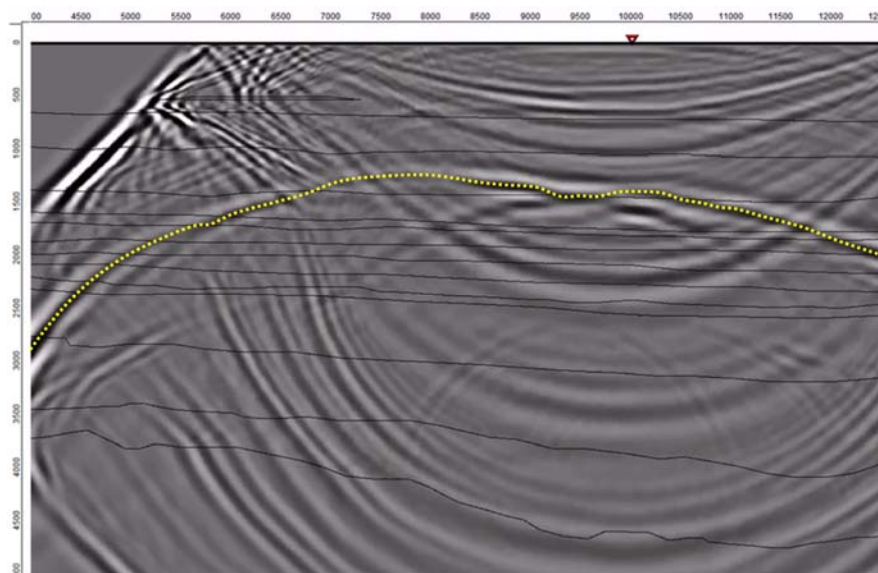


Figure 59. Snapshot of the propagating wave field generated by a shot in the good data area.

Figure 59 shows one snapshot of the wave field generated by a source point located 10,000 meters from the left edge of the model (in the good data area). The wave front has propagated through all layers to the base layer and is now reflecting upward toward the receivers at the surface. Concave waves are downward propagating and convex are upward propagating. We have highlighted the basement reflection with a dashed yellow line. Clearly the reflection is travelling to the surface through a relatively quiet part of the wave field. The signal to noise ratio is very good and that reflector will be clear on the resulting recorded data.

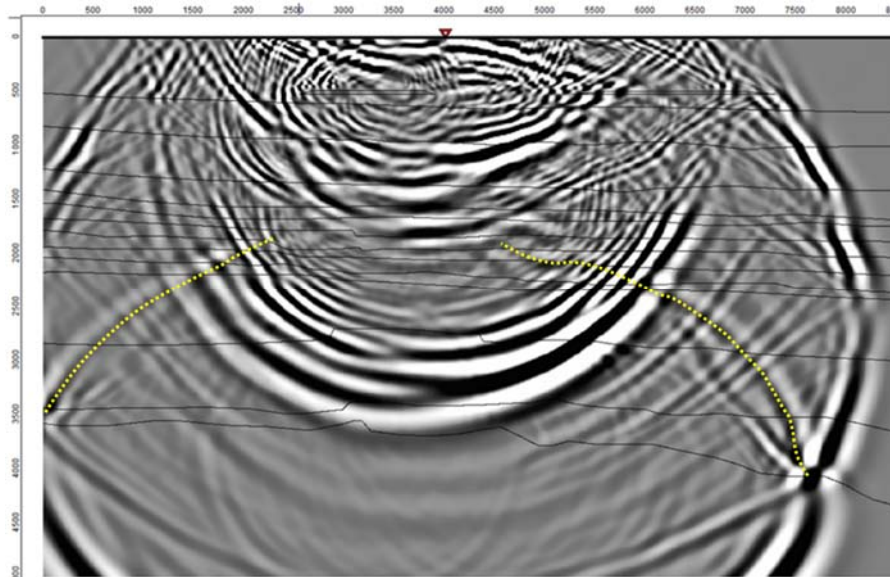


Figure 60. Snapshot of the propagating wave field generated by a shot in the bad data area.

In figure 60, we show a snapshot of the wave field generated by a source point located 4000 meters from the left edge of the model (in the bad data area). Due to energy loss through the shallow basaltic sills, the basement reflection (highlighted by the dashed yellow line) is much weaker. Also, the edges of the erratic sills have acted as Huygens scattering points and have generated high amplitude reverberating noise in the shallow section. As the weak deep reflection tries to make its way to the surface, the signal to noise ratio is drastically reduced due to the strong near-surface scattered wave field.

Now try to imagine this process where there are many more sills. Not just in a 2D section, but also edges and boundaries of erratic sills all around the source in a 3D world !! So much scattered energy will interact chaotically and will appear at the surface as chaotic patterns. This will form chaotically-scattered source-generated noise somewhat like that in figure 26 but much worse in magnitude compared with deeper reflection signals.

Chaotically-scattered source-generated noise can appear like random noise in many domains. The difference between random noise and this noise is that source-generated noise is not time variant. It is repeatable every time a source is repeated from the same source location and observed from the same receiver locations. Also, most time-variant random noise (such as wind) is relatively low in magnitude (a few tens of microvolts as measured on many conventional instruments). Source-generated near-surface noise is very strong in magnitude (a few tens of millivolts or more). Source generated noise can easily be 60 decibels stronger than typical random noise.

Figure 61 shows data collected from two areas from the processed data volume. These are super gathers. They are traces from a range of adjacent bins small enough so that the geology does not change significantly over the area but large enough so that a large number of diverse offsets are collected. These super gathers are almost completely populated with offsets at a small and slightly irregular offset interval. The data has been processed through gain, normal move-out correction, statics corrections, deconvolution and some noise suppression.

In the good data area (data on the right in figure 61), we can clearly see good quality reflections (flat events in a CDP gather). We also see a fairly strong air blast running steeply downwards through the near offsets. In the bad data area (left side of figure 61), we see what mostly appears to be random noise. In fact it is chaotically-scattered source-generated noise. We also see the strong air blast. Because the air blast propagates above the surface of the earth, it is not effected by the scattered waves that exist not far below the surface of the earth. Unfortunately, the air blast is about the only coherent signal we see in the bad data area and it contains no information about the sub-surface geology.

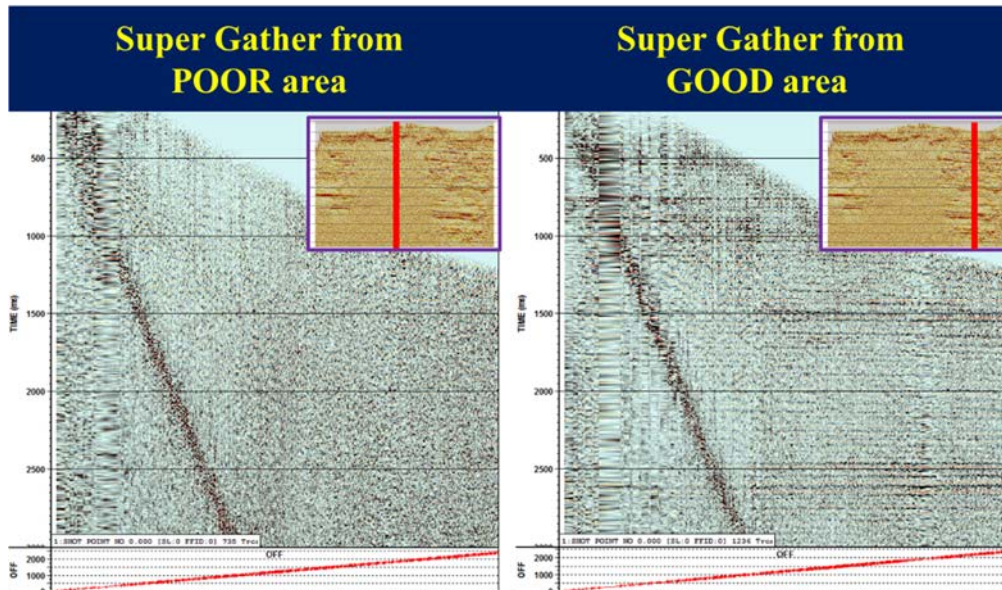


Figure 61. Comparison of a CDP super-gather from the poor data area versus the good data area.

Using our “Data Simulation” software, we can use these super gathers to simulate stacked data volumes for a variety of 3D models. Figure 62 shows a reference super gather in the top left. We compare that to the offset distribution predicted for one bin from a 3D computer model. The super gather shows us one sample of the signal and noise conditions from an existing 3D program. The computer model shows us the geometrical statistics for a set of parameters considered for the next 3D program.

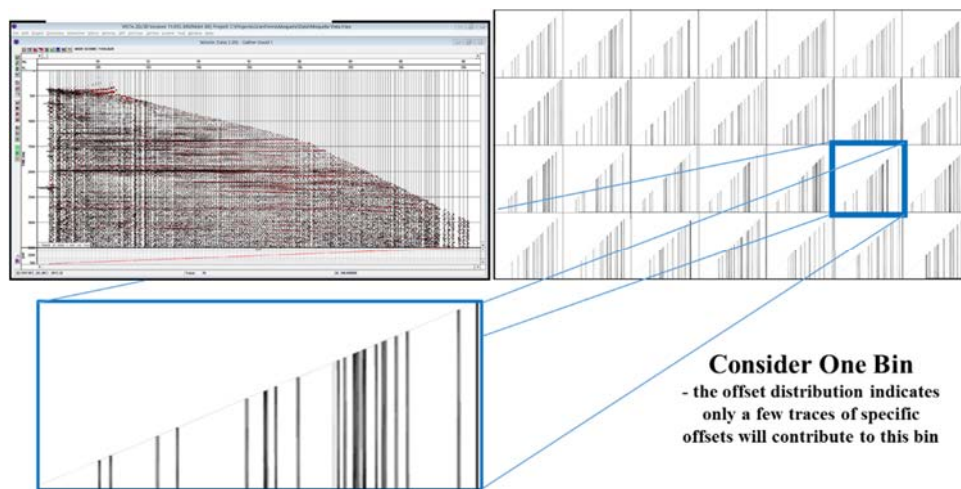


Figure 62. Comparison of a CDP super-gather with the offset distribution for one bin predicted from a 3D model.

Figure 63 shows that we select only the traces from the reference super gather that correspond to the offsets described for that bin by the model. We stack that subset of traces to create one stacked trace for that bin.

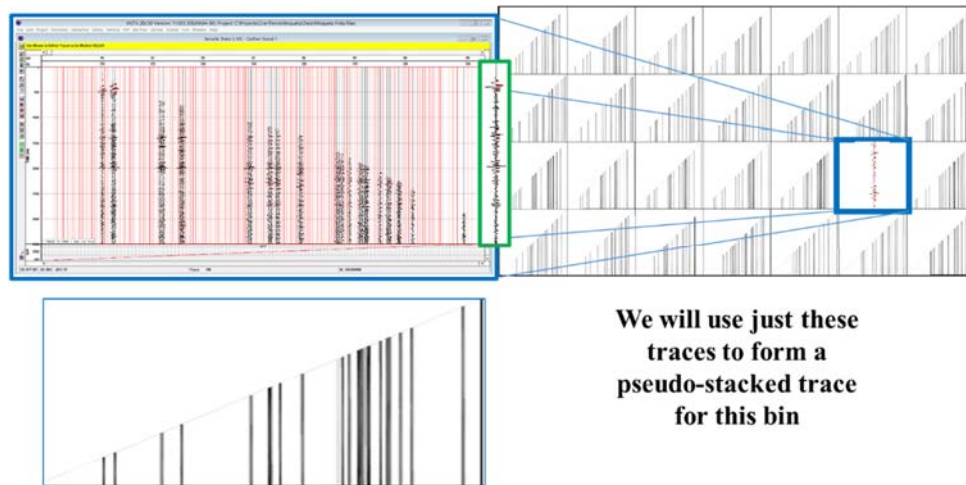


Figure 63. We select just the traces from the reference super gather that correspond to the expected offsets in the model bin, average them to form one stacked trace and put that trace in the corresponding bin location in a 3D volume.

We then repeat the process for each bin in the model. Each stacked trace will be unique to the extent that we are selecting a different sub-set of traces from the reference super gather. Eventually, we create a full synthetic 3D data volume that can be viewed in any 3D interpretation software. Since all traces are simulated from the same reference super gather, the 3D volume will show no variation due to geology. Any trace-to-trace variation in the simulated volume will be entirely due to the bin-to-bin offset variations of the 3D model combined with the changing nature of the reflection signal and noise with offset in the super gather.

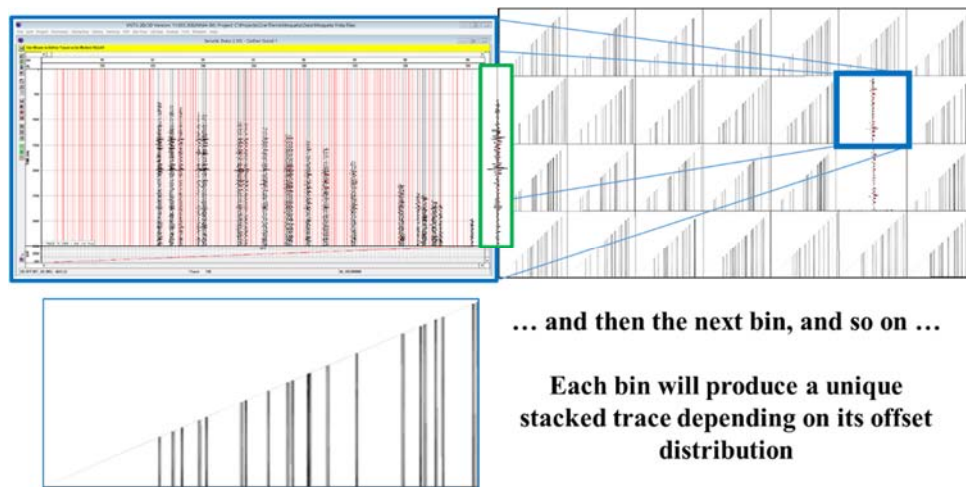


Figure 64. The next bin generates a different set of offsets, so the stacked trace consists of a different sub-set of traces from the reference super gather.

We used data simulation to compare the anticipated results for models of higher density compared to the original parameters that resulted in the data shown in figure 57. The following table shows the parameters for the original survey plus the three models we evaluated.

		Mustagh Dense	Mustagh Moderate	Mustagh Sparse	Original Parameters
Receiver Interval (m)		36	42	48	50
Source Interval (m)		36	42	48	50
Receiver Line Spacing (m)		72	126	192	250
Source Line Spacing (m)		108	168	240	350
Receiver line sparcity		2.0	3.0	4.0	5.0
Source line sparcity		3.0	4.0	5.0	7.0
Box Aspect Ratio	SL / RL	1.500	1.333	1.250	1.400
Receiver point density (per sq km)		385.80	188.96	108.51	80.00
Source point density (per sq km)		257.20	141.72	86.81	57.14
Receiver line density (km / sq km)		13.89	7.94	5.21	4.00
Source line density (km / sq km)		9.26	5.95	4.17	2.86
Active Patch lines		48	28	18	10
Active Patch stations		120	104	100	98
Useable offset (EI Trebol) (m)		680	680	680	680
Natural fold (EI Trebol)		46.70	17.16	7.88	4.15
Trace Density (EI Trebol) (per sq km)		144,147	38,904	13,683	6,641
Useable offset (M7) (m)		1,670	1,670	1,670	1,670
Natural fold (M7)		281.69	103.48	47.53	21.39
Trace Density (M7) (per sq km)		869,404	234,641	82,525	34,223
Useable offset (D129) (m)		2,400	2,400	2,400	2,400
Natural fold (D129)		461.01	173.31	81.47	32.67
Trace Density (D129) (per sq km)		1,422,883	392,993	141,435	52,265

Figure 65. Parameters for three models more dense than the original survey.

Using the super gather from the good data area, we simulated the sparse, moderate and dense models. Figure 66 shows a typical in-line slice from each of the three simulated data volumes. The cost estimate for each model over the planned survey area would be approximately \$10 million, \$14 million and \$23 million respectively. Certainly we see improvement in the stacked data quality using the dense parameters (right side of figure 66) versus the sparse parameters (left side). However, it would be hard to justify the extra cost just for this level of improved imaging. The data on the left is interpretable and would be sufficient for mapping structure and significant stratigraphic changes. It is likely that the data on the right would be more suitable for subtle stratigraphic plays and studies involving pre-stack attributes and rock properties.

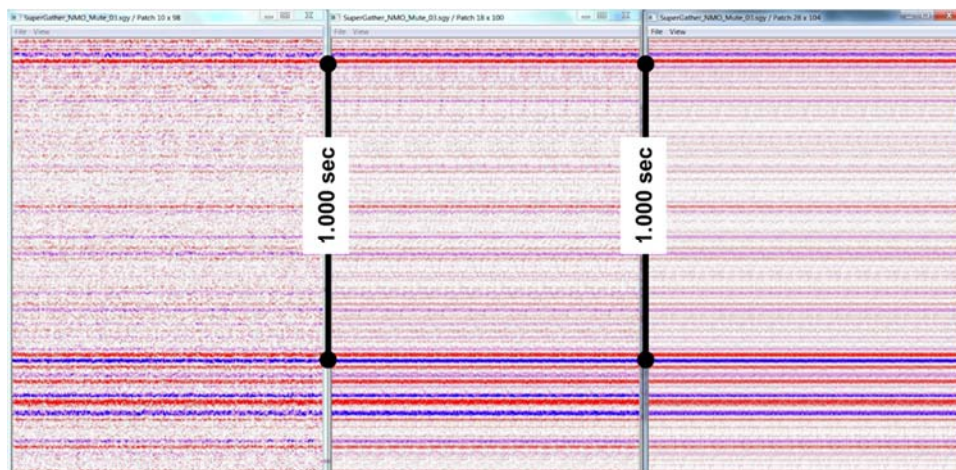


Figure 66. Data volumes predicted using the good data super gather for three models.

In figure 67, we show the same in-line slices from data volumes for the same three models but using the poor quality super gather. This is how we may expect the respective 3D surveys to look in the poor data area. In this case, it is obvious that a denser grid is necessary in order to better sample and suppress the strong noise.

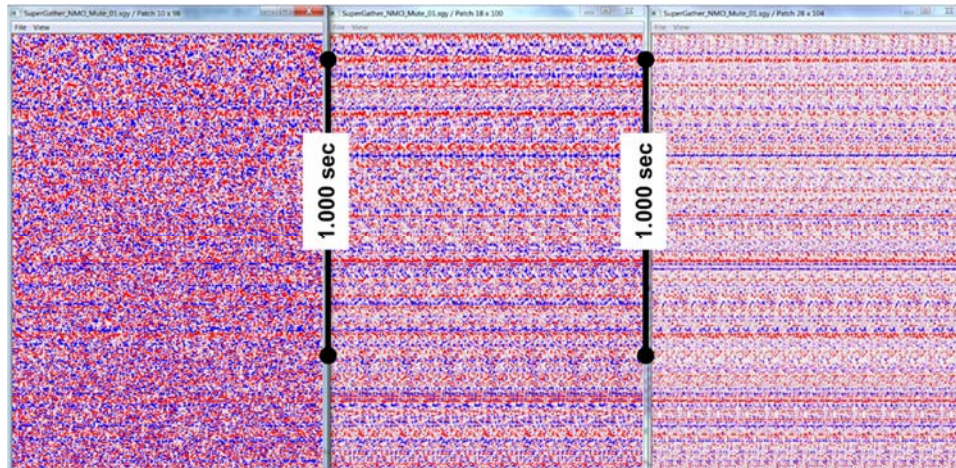


Figure 67. Data volumes predicted using the bad data super gather for the same three models.

Increasing trace density by reducing source and receiver intervals along original lines will increase the total recorded trace count. However it is not very effective for increasing the offset and azimuth diversity within each bin.

Increasing trace density by decreasing source and receiver line spacings is a much better method because it adds more traces to each bin and maximizes statistical diversity amongst those traces. In the preceding example we demonstrated data quality improvement by reducing both station intervals and line spacings.

In the presence of strong chaotically-scattered source-generated noise, it is important to have high trace density but particularly important that statistical diversity is maximized amongst those traces.

Final Comments

In the first part of this paper we described the concept of apparent wavelengths as a reflected wave field emerges against a flat recording surface. We discussed spatial sampling and aliasing of signals. Most design processes allow us to calculate the largest spatial sample interval that will properly measure all components of our desired reflection signals. Sometimes, we do not pay proper attention to diffracted signals or noise contributions.

We then identified several unique types of noise that we encounter in seismic data including:

- Random noise (time variant and Gaussian distributed in amplitudes)
- Erratic (such as traffic, culture and industrial noise)
- Noise due to irregular source behavior
- Coherent source-generated noise
- Chaotically-scattered source-generated noise

Random noise is generally weaker in average amplitude compared to the others. Properly measured coherent noise modes are generally best dealt with in processing. Random noise, erratic noise and chaotic noise can be quite broadband in wavelength.

In our experience, the worst offending noise is some type of chaotically-scattered noise. Common places where this occurs is in ancestral valleys of meandering rivers, areas with Karstified surfaces, areas with high velocity layers at or near the surface and areas of rugged surface topography.

Noise that includes short wavelength components is usually not sufficiently measured with designed spatial sample intervals. In such cases it is necessary to sub-sample our source and receiver intervals. This may be accomplished by using single-sensor and single-source components at intervals that should be about 1/3 of conventional intervals (or less). It may also be accomplished with the use of source and/or receiver arrays. However the arrays should be kept quite short in order to limit the attenuation due to differential arrival times that may be due to NMO or in-group statics.

Most often, well designed short arrays coupled with forced mid-point scatter such as the triple-stagger design are more cost effective than discrete sub-sampling.

Many papers have been presented or published regarding the use of arrays. Yajaira Herrera did a review of array publications as part of her Master's degree in 2004. It was interesting to note that only a few papers on arrays were published from 1960 to 1990 and most of those were in favor of arrays. Generally, these were prepared by oil company research departments and independent consultants.

From 1990 to 2000 Input-Output and Sercel were trying to sell their digital MEMS sensors and there was a dramatic increase publications about arrays. They were almost all anti-array. Of course, these papers were prepared or sponsored by Input-Output or Sercel and the prime motivation was to sell their single-sensor products. They were not very objective. As independent experts on arrays, it was very transparent that the papers presented one-sided information selected to favor their single-sensors.

In 2000 Western Geco rolled out the public release of their Q-Land recording system at the SEG Convention (held in Calgary that year). They presented many papers showcasing their product where individual analog geophone accelerometers (GACs) were recorded. These were point-receivers. However, instead of one recorded channel every 50 meters, they used one GAC (one recorded channel) every 6.25 meters (i.e. 8 times the recorded channels). In conjunction Delft University, Netherlands coincidentally presented several papers showing how analog arrays could be destructive to data. Again, these papers were sponsored by a company with a vested interest in convincing people that it was necessary to record individual elements at small spacing as discrete channels rather than averaging them in the field with analog arrays. Most of Delft's anti-array papers were quite contrived and used examples of very poor array design.

In Yajaira's review, she found that if you discarded the commercially motivated papers, then there was only a mild increase in the number of publications about arrays since 1960. Some of those are well researched and well written, some are easily identified as poor quality work. And both categories offer both pro-array and anti-array conclusions.

Most of the papers that are negative towards arrays will start with the comment that the purpose of arrays is to suppress ground roll or air blast. If you see that comment in a paper, it is an indication that the author does not understand array theory very well. As we have pointed out, arrays must be designed to pass signal, not only to eliminate noise. The problem with attacking ground roll or air blast with arrays is that these noise modes have a range of wavelengths that overlaps signal. If you make an array long enough to attenuate ground roll, it will definitely also attenuate some important wavelengths of signal. Another common problem is that people use receiver intervals that are too long to properly sample the desired wavelengths of signal. Then they match the array length to the receiver interval. When the results are bad, they blame the array. In general (at least in 2D programs), if an array length equal to the receiver interval is damaging to the data, the problem is probably not the array, but rather that the chosen receiver interval was inappropriate to the objectives of the program.

Most of the studies that were well conducted often conclude that arrays are not destructive to the data, but neither were they helpful. Therefore, these papers conclude that arrays are unnecessary. And for the project areas that were studied, those conclusions are absolutely correct. When you examine the data quality where these studies were done, it becomes obvious that the area produces very good data with no chaotically-scattered source-generated noise. If such noise is not prevalent, then there is no need for arrays. However, where this noise is a significant factor, it is absolutely necessary to sub-sample the returning wave-field by reducing the spatial sample interval. We can show many examples where this noise is present and data recorded with analog arrays is superior to data recorded at conventional receiver intervals with point receivers. Instead of arrays, you can choose the Q-Land strategy and place individual point receivers with a spacing similar to the geophone

spacing within an array (typically less than or equal to one third of the normal receiver interval). Either solution can be helpful, but cost and operational considerations must also be considered. For example, in urban areas, we often forego the use of arrays in order to limit the visibility of our operations and to minimize disruption to local residents. But we try to compensate by using carpet-receiver methods and higher density designs.

With regard to the use of arrays, there are definitely differences of opinion amongst some of our leading experts. Very simply, you should not expect one answer that is always correct. There are areas to use arrays and there are areas to forego them. There are arrays that are beneficial when coordinated with spatial sub-sampling methods (generally very short arrays) and there are arrays that are poorly planned that can be detrimental to data (generally long arrays). What is long and what is short in arrays is very much a function of project targets and objectives.

We hope you find this dissertation informative and useful. Please feel free to distribute it to associates if you wish, but please distribute the entire document (do not provide selected excerpts). Also, please ensure that Mustagh Resources Ltd. is recognized as the original author.

Best Regards,
Norm and Yajaira

Norm Cooper, P.Geoph., President
Yajaira Herrera-Cooper MSc, Geophysicist
Mustagh Resources Ltd.
134 Hubman Landing
Canmore, Alberta, Canada
T1W 3L3
Phone: (403) 265-5255
Fax: (403) 609-3877
Cell: (403) 680-6676
ncooper@mustagh.com
www.mustagh.com

Please consider your environmental responsibility before printing this document